SIMULATION AND OPTIMISATION OF GAS STORAGE TANKS FILLED WITH CAPACITANCE

WILHELMUS JOHANNES VAN ROOYEN

B.ENG. (MECHANICAL)

MINI-DISSERTATION SUBMITTED IN PARTIAL FULFILMENT OF THE REQUIREMENTS FOR THE DEGREE

MAGISTER ENGENERIAE (MECHANICAL ENGINEERING)

SCHOOL OF MECHANICAL AND MATERIALS ENGINEERING

AT THE

POTCHEFSTROOM UNIVERSITY FOR CHRISTIAN HIGHER EDUCATION

Promoter: Prof. E.H Matthews

Potchefstroom

2003

ABSTRACT

The Pebble Bed Modular Reactor (PBMR) is a revolutionary small, compact and safe nuclear power plant. It operates on a direct closed Brayton cycle. One of the unique features of this concept is its load following capability enabled by extracting or injecting helium from or to the system during operation.

This characteristic of the PBMR requires that extracted helium must be stored during load following periods. When more power is required from the system, this stored helium can be injected into the system again. The attempt to make the PBMR as small and compact as possible ended up in problems with large storage tanks.

A proposal was made to fill the tanks with heat capacitance. This would reduce the necessary gas storage area dramatically. Helium is injected in to the tanks at 120°C. The capacitance would absorb the energy that the gas contains and consequently the gas would experience a decrease in temperature. This implies that the density of the gas will increase and result that more helium can be stored in the same tank before the tank's maximum operating pressure is reached.

A Computational Fluid Dynamics (CFD) simulation was done to determine how feasible the proposal was. The simulation showed that the capacitance reduced the total pressure in the tank significantly. This implied that more helium can be stored in the same tank or that a smaller tank can be used to store the same mass of helium.

The large heat transfer area that the capacitance provides result that this kind of system has a quick thermal response. Since, the system experiences short injection periods (60 seconds), it is a very useful characteristic. In order to make optimal use of this advantage, the gas must be distributed evenly throughout the tank and no local high temperature regions must occur in the tank. A few injection concepts were investigated in order to optimise for this requirement.

UITTREKSEL

Die Kieselbed Kern Reaktor (KKR) is 'n revolusionêre klein, kompakte en veilige kern aanleg. Dit word aangedryf deur middel van 'n direkte geslote Brayton siklus. Een van die unieke kenmerke van hierdie konsep is die vermoë om kraglewering te reguleer soos wat die elektriesiteitsaanvraag varieer gedurende bedryfstoestande.

Hierdie eienskap van die KKR vereis dat helium gedurende periodes met lae aanvraag, uit die siklus onttrek en gestoor moet word. Indien meer krag benodig word, word helium teruggeplaas in die stelsel. Die poging om die KKR so klein en kompak as moontlik te maak, het probleme veroorsaak met groot bergingsreservoirs.

'n Voorstel is gemaak om die reservoirs te vul met 'n hitte kapasitansie. Dit sou die nodige volume om helium in te berg, drasties verklein. Helium word in die tenk gepomp teen 120°C. Die kapasitansie absorbeer die energie wat hierdie helium bevat. Sodoende verlaag die temperatuur van die gas. Dit impliseer dat die digtheid van die gas toeneem, en gevolglik kan daar meer helium in die tenk geberg word voordat die maksimum ontwerpsdruk van die tenk bereik word.

'n Berekenings Vloei Meganika (BVM) simulasie is gedoen om te bepaal hoe lewensvatbaar hierdie voorstel was. Die simulasie het getoon dat die kapasitansie 'n merkwaardige verlaging in die totale druk van die tenk tot gevolg gehad het. Dit het geïmpliseer dat meer helium in 'n tenk met dieselfde volume gestoor kon word, of alternatiewelik kon 'n kleiner tenk gebruik word om dieselfde massa helium te berg.

Die groot hitte oordrag area wat die kapasitansie verskaf, bring mee dat hierdie stelsel 'n vinnige termiese reaksie het. Dit is 'n baie handige eienskap van die stelsel omdat helium vir kort tydperke in die tenks ingepomp word (60 sekondes). Om optimale gebruik van hierdie voordeel te maak, moet die helium eweredig deur die hele tenk versprei word. Dus moet daar geen lokale hoë temperatuur gebiede voorkom nie. 'n Paar verskillende konsepte in hierdie verband is ondersoek om die stelsel te optimeer vir hierdie vereiste.

TABLE OF CONTENTS

LIST OF ABBREVIATIONS

CFD	Computational Fluid Dynamics
HVAC	Heating, Ventalation and Air Conditioning
ICS	Inventory Control System
NNR	National Nuclear Regulator
PBMR	Pebble Bed Modular Reactor (The unit, The Project or The Company)
PCU	Power Conversion Unit
PU for CHE	Potchefstroom University for Christian Higher Education

LIST OF FIGURES

LIST OF TABLES

1. INTRODUCTION

1.1 BACKGROUND

The increasing demand for energy in the world created a large research field in finding economical ways to convert energy into electricity. Nuclear power was always considered as a potential solution to the problem, although questions regarding its safety are always raised along with this concept.

Small, safe, clean, cost-effective and adaptable - These are the features of the Pebble Bed Modular reactor (PBMR). South Africa's power utility giant, Eskom, has committed itself to the development of the PBMR so that it can be part of the future energy provision network of the world.

The nuclear technology of the PBMR is based on a concept that was developed in Germany by Prof. Dr. Schulton. Silicon carbide-coated uranium granules are compacted into hard billiard-ball-like spheres (Figure 1) to be used as fuel for a high-temperature, helium-cooled gas reactor [1].

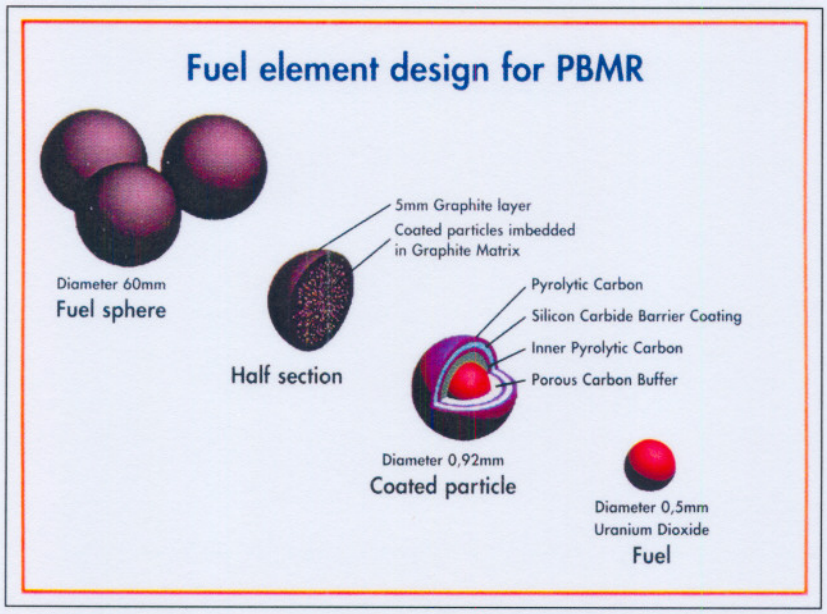

Figure 1: A presentation of the pebble fuel design.

This concept was transformed into a design that resulted in the AVR ("Arbeidsgemeinschaft Versuchsreactor"), a 15 MW (megawatt) demonstration pebble bed reactor, built in Germany. It operated successfully for 21 years, but the intense wave of post-Chernobyl anti-nuclear sentiment that swept Europe brought an early end to this reactor [1].

Eskom started with feasibility studies regarding the possibility of PBMR's being built in South Africa in 1994. The design and costing studies showed that the PBMR has a number of advantages over other potential power sources [2].

It is highly competitive to all kinds of energy. Most of South Africa's coal-fired power stations have to be built near the pit-heads of coal-producing areas. This requires long power lines from coal-rich areas, where the pit-heads are situated, to the load centres. This implies high capital costs and transmission losses. The alternative option of transporting coal to distant power stations is unfeasible.

The opportunities in South Africa for producing hydro-electric, or power for natural gas, is limited. Large thermal, nuclear or hydro-electric power stations also require lead times of up to eight years and could result in the installation of surplus capacity if economic growth is not expected [2] .

Eskom experiences short, sharp, demand peaks in winter that is difficult to accommodate with the slow ramping characteristics of the existing large power stations. Every modern utility will pay a premium for plants with load following capability. Not only does it provide the utility with the ability to meet all power demands (base and peak load) with the same plant, but there are also hefty premiums attached to peak load supply [1].

These factors created the need for small electricity generation units situated near the points of demand. The PBMR concept, which has a relatively short construction lead-time, low operating cost and fast load following characteristics, is such an option. Plus, the pebble fuel used in this concept has inherently safe characteristics.

Research showed that a closed loop Brayton cycle layout with a three-shaft configuration would provide the optimal thermal efficiency for the PBMR. Figure 2 shows a simplified schematic diagram of the working of a Brayton cycle; the working of the cycle is stepwise described below [3].

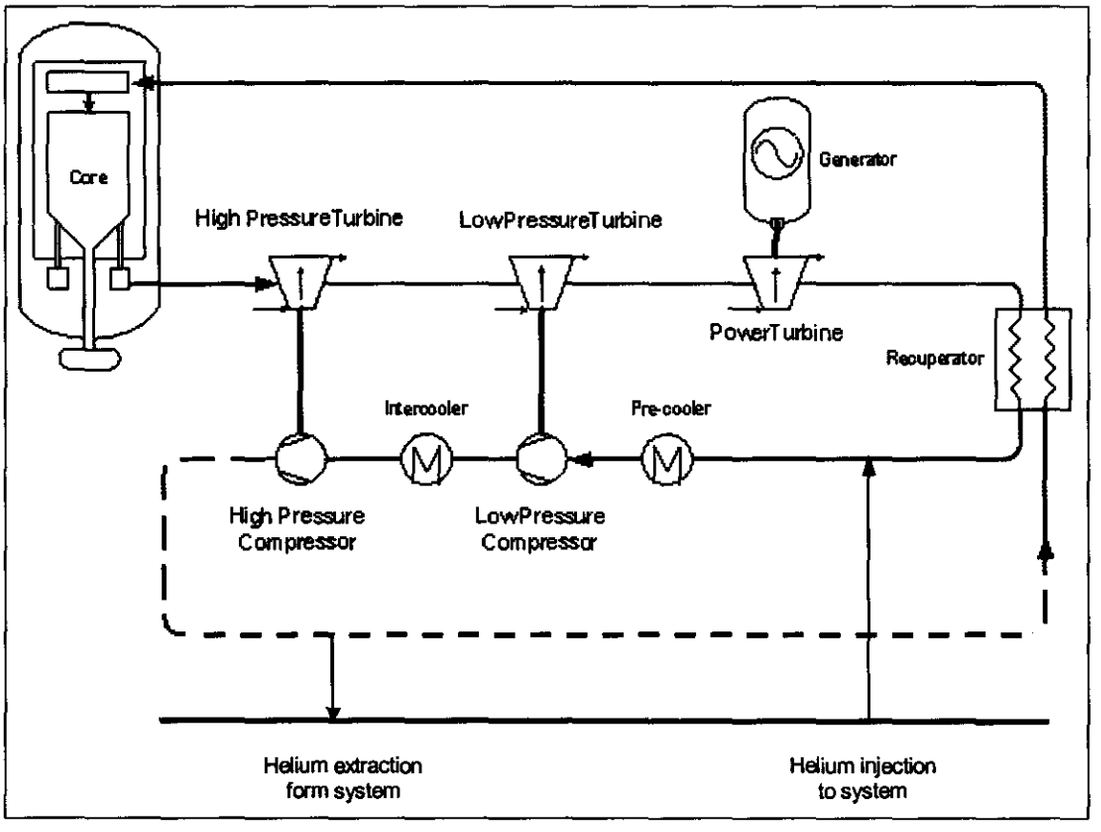

Figure 2: Simplified diagram of a direct Brayton cycle nuclear power conversion system.

Helium enters the reactor at a temperature of about 500 °C and a pressure of 8.6 MPa [4]. It is conveyed to the top of the reactor via annular riser channels. The gas then moves downward through the fuel spheres. During this process helium absorbs heat from the fuel spheres, which were heated by the nuclear reaction. The heated gas leaves the reactor at a temperature of about 900 °C.

The reactor outlet is connected to the High-pressure Turbine, which forms part of the High-pressure Turbo unit. The High-pressure Turbine drives the High-pressure Compressor.

Next, the helium flows through the Low-pressure Turbine, which drives the Low-pressure Compressor; this unit is known as the Low-pressure Turbo unit. The Low-pressure turbine outlet is connected to the Power Turbine. This turbine drives the generator.

After the helium exits the Power turbine it is still at a high temperature. During the next step of the cycle the gas flows through the primary side of the recuperator where its heat is recuperated to the helium entering the reactor (refer also to the last step of the process).

After the gas exits the recuperator, it is further cooled by the pre-cooler before passing through the Low-pressure compressor. If the gas is cooled before the compression process, the increase in density results in a more efficient compression process.

The outlet of the Low-pressure compressor is connected to an Inter-cooler where the gas is cooled before entering the High-pressure compressor. This compressor compresses the helium to 8.7 MPa. The cold (±100°C), high-pressure helium then flows through the recuperator where it is pre-heated before it returns to the reactor.

A three-shaft recuperative Brayton cycle was never physically tested before and there was much scepticism surrounding this concept. It was labelled as an unstable cycle that won't be self-sustaining or controllable. In order to address the scepticism, a test rig that operates on this cycle was built at the PU for CHE in 2002 (Figure 3). The project was a success and proved that this concept is feasible; the cycle bootstrapped and could be controlled [5].

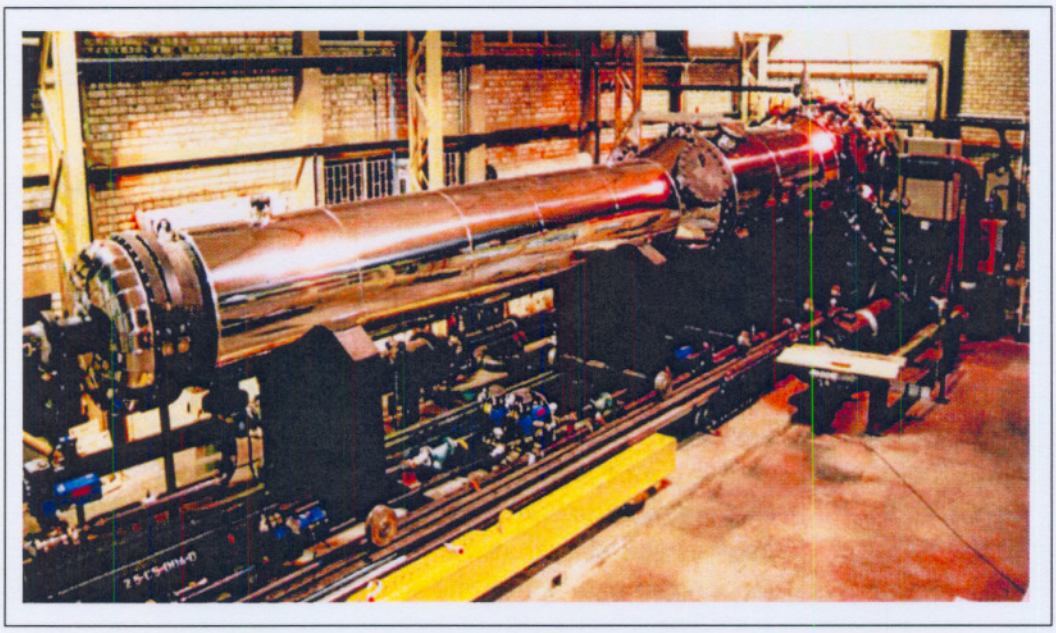

Figure 3: The test rig that were built at the PU for CHE

In order to do load following with a Brayton cycle, helium is extracted or injected from or to the system, respectively. The system responsible for load following of the plant is known as the Inventory Control System (ICS), while the tanks where the helium is stored after extraction from the system is known as the Inventory Control System tanks (ICS tanks). Refer to Figure 4.

Figure 2 shows the areas in the system where injection and extraction of helium takes place. Extraction from the system takes place at the position of highest pressure (after the High-pressure compressor) while injection takes place at the position of lowest-pressure (Downstream side of the Low-pressure recuperator). The reason for injecting and extracting at these specific positions is to minimise the use of external pumps or compressors and the ICS tanks by utilising the pressure difference within the Power Conversion Unit (PCU) [6].

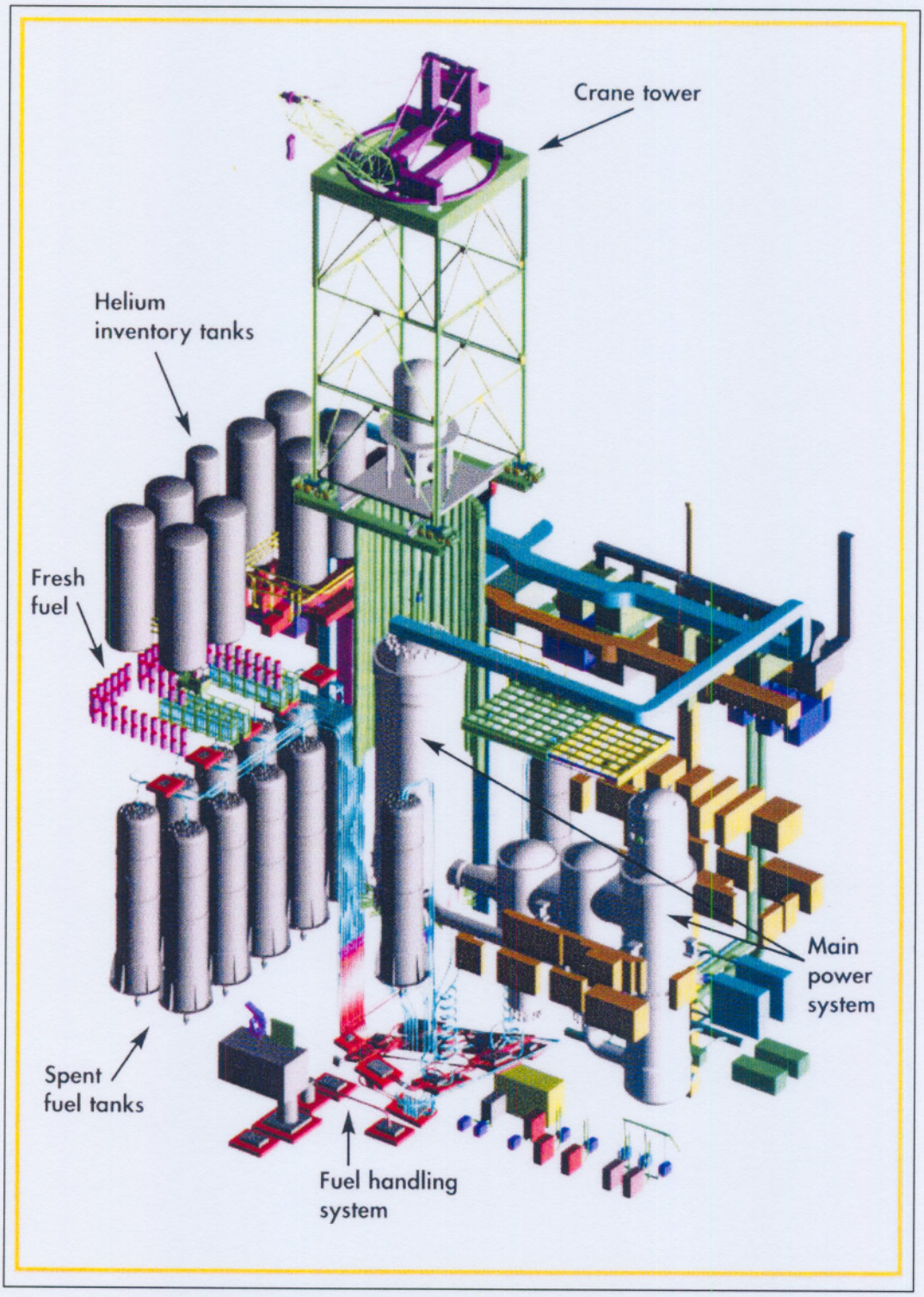

Figure 4: Layout of the PBMR

1.2 PROBLEM STATEMENT

To perform the mentioned load following, large storage tanks are required for the extracted helium. After investigation a method was proposed to reduce the size and hence the volume of the helium storage tanks, decreasing the cost of the ICS tanks.

The proposal entailed the filling of the tanks with a woven steel mesh, similar to steel wool. This should increase the heat capacitance of the storage system and decrease the size [7]. When helium is injected into the tanks, the capacitance absorbs energy form the gas; decreasing the helium internal energy. A decrease in energy will result in a decrease in temperature of the gas with a subsequent increase in the gas density. This implied that a smaller tank would be necessary to store the same amount of helium.

The possible reduction in the ICS storage tank volume resulting from the proposal had to be quantified. An appropriate and economical method had to be found to determine how efficient and feasible this suggestion was.

1.3 LITERATURE REVIEW OF CONCEPT

As mentioned, it was expected that the capacitance would cool the gas by absorbing some of the thermal energy of the injected helium. It would act as a passive cooling device, which implies that no external driving source is used in this process. The thermal energy initially contained in the injected gas will be stored in the capacitance.

A decrease in the helium temperature would increase the average density of the gas. An increase in the gas density results in a lower total pressure in the tank after a certain injection period at a constant mass flow rate, than if no capacitance was used. Helium at a temperature of 120°C is injected into one of the tanks at 9 kg/s for a period of 60 seconds. The initial pressure and temperature in this tank is 3019.0 kPa and 20°C, respectively.

Pressure vessels are designed for a specific operating pressure, which means that the total pressure inside the tank must under no circumstances exceed this value. If the total pressure inside the tank can be decreased it implies that more gas can be stored in the tank. Another possibility is that a smaller, cheaper tank can be used to store the same mass of gas.

The concept of using some kind of porous media in heat exchangers or thermal storage systems is commonly used in industry. Most popular is the packed bed concept, where the vessel is filled with spheres [7].

The major advantage of this concept is that the porous media provides a large heat transfer area [9], which is of great importance when designing components in this regard. A large heat transfer area improves the convective heat transfer from the gas in the solid material.

The large surface-to-volume ratio also results that this system has a relative fast thermal response compared to other developed energy carrier devices [10]. This is a very useful characteristic of these kinds of thermal storage systems; quick response from the ICS results in shorter gas injection periods.

This characteristic of the system makes it ideal for the current application. The load following capability of the plant requires a storage system that can cool and store large volumes of helium in a short time.

Another important aspect to consider is the thermal conduction capability as well as the specific heat of the porous material. Literature showed that these two material properties are dominant factors when designing this kind of heat exchanger [11].

It is evident that the thermal conductivity of the capacitance is important for the conduction of heat from the surface of the solid material. The specific heat gives an indication of the amount of thermal energy the medium can store for a specified temperature increase during transient scenarios. More energy stored in the capacitance results in a lower final average gas temperature.

There are materials available with better thermal conductivity and specific heat characteristics than steel, but the costs involved in these options must be considered. Steel wool is an off the shelf item that is easily available and not expensive. The capability of steel wool to act as a dust filter was an added advantage, but this report won't elaborate on this.

Convection and conduction are the two heat transfer mechanisms that dominate in a porous heat transfer field [12]. The contribution of radiation to the total heat transfer in a porous media at low temperatures is insignificant [13]; therefore the simulations were done without modelling radiation.

Thus, from a literature survey conveyed on the concept it appeared that it is commonly used in industry. The large surface area of the porous medium improves the convective heat transfer between the gas and the solid material. It enables the porous medium to absorb large amounts of the energy (that is contained in the gas) in a short time. All of the information from the literature survey merits the investigation of the proposal.

1.4 OVERVIEW OF REPORT

The first section of the report elaborated on the background of the plant as well as the proposed concept. A literature survey was performed to understand the working principle as well as important aspects to consider when designing such a system.

The next two sections discuss the selected solving approach in detail as well as how the different aspects of the concept was implemented and addressed in the solving technique. Section 2 is a detailed literature review on the solving method, while Section 3 discusses the implementation of the chosen solving method.

The following chapter discusses the interpretation and verification of the results. It was important to verify the results in order to ensure that the selected solving approach as well as all the assumptions made, were accurate. The last part of this chapter is used to investigate the possibility of optimising the current concept.

The last two sections of the report contain the conclusions that were made out of the study, as well as a list of all the references that were used to conduct the study. Recommendations for future work in this regard are also given.

2. SELECTION OF AN APPROPRIATE SOLVING METHOD

2.1 PREAMBLE

A few different approaches can be considered to solve this kind of fluid flow scenario. Building an experimental set-up and testing the concept would obviously have provided reliable answers; but if the time and costs involved in such an experiment are considered, it is totally unfeasible.

Solving this problem with an analytical approach out of first principles is also very complex and optimistic. A numerical approach, such as CFD (Computational Fluid Dynamics) would be far more appropriate. There are many CFD software codes available on the market for simulation purposes. However, most of them work on the principle of solving the Navier-Stokes equations with appropriate boundary conditions.

Another possibility was also to use a network approach. This method also solves the Navier-Stokes equations, but the equations are simplified in such a way that only one flow dimension is solved [14]. A flow network is built with different elements, where it is still possible to solve a multi-dimensional flow field by using various elements to present flow in different dimensions. Many assumptions is involved in applying this method which would still make CFD more appropriate.

The ultimate goal of a CFD simulation is to understand the physical phenomena in the flow of fluid as well as heat transfer around and within designed objects. It should be clear that the success of CFD simulations is highly dependent on the implementation of a range of issues; from grid generation and turbulence modelling to the applicability of various simplified forms of the Navier-Stokes equations [15].

If CFD is used for the correct application and implemented correctly, it is a very elegant way of solving complex fluid flow scenarios. This chapter will give a theoretical background on CFD. The methodology of solving any problem relating to CFD will also be discussed.

2.2 BACKGROUND ON CFD

The field of CFD has a broad range of applicability. Regardless of the specific application studied, the following sequence of steps [15] must generally be followed to obtain a satisfactory solution.

2.2.1 PROBLEM SPECIFICATION AND GEOMETRY PREPARATION

The first step involves the problem specification, including the geometry, flow conditions, and the simulation requirements. The geometry may result from an existing configuration or may be associated with a design and optimisation study.

Alternatively, in a design context, no geometry are supplied. Instead, a set of objectives and constraints are specified. Flow conditions might include, for example, the Reynolds number and Mach number for the flow over an airfoil.

The simulation requirements include issues like the level of accuracy required, the required turnaround time, and the solution parameters of interest. Unfortunately accuracy and turnaround time are usually conflicting and a compromise is necessary.

2.2.2 SELECTION OF GOVERNING EQUATIONS AND BOUNDARY CONDITIONS

Once the problem has been specified, an appropriate set of governing equations and boundary conditions must be selected. It is generally accepted that the phenomena of importance to the field of continuum fluid dynamics are governed by the conservation of mass, momentum and energy.

The partial differential equations resulting from these conservation laws are referred to as the Navier-Stokes equations. However, in the interest of efficiency, it is always prudent to consider solving simplified forms of the Navier-Stokes equations when these simplifications retain the physics that are essential to the aim of the simulation.

Possible simplified governing equations include the potential-flow equations, the Euler equations and the thin-layer Navier-Stokes equations. These may be steady or unsteady and compressible or incompressible. Boundary types that may be encountered include solid walls, inflow and outflow boundaries, periodic boundaries, symmetry boundaries etc.

The specification of boundary conditions is strongly dependent on the selected governing equations. For example, at a solid wall, the Euler equations require flow tangency to be enforced, while the Navier-Stokes equations require the no-slip condition. The success of a simulation depends greatly on the engineering insight involved in selecting the governing equations and physical models based on the problem specification.

2.2.3 SELECTION OF MESHING STRATEGY AND NUMERICAL METHOD

Next a numerical method and a strategy for discritizing the flow domain into cells, or elements, must be selected. Most of the CFD software codes available on the market only use numerical methods; these methods require a tessellation of the domain, which is known as a grid, or mesh.

Many different meshing strategies exist, including structured, hybrid, composite, and overlapping meshes. Furthermore, the mesh can be altered based on the solution in an approach known as solution-adaptive meshing. The numerical methods generally used in CFD can be classified as finite-difference, finite-volume, finite-element, or spectral methods.

The choices of a numerical method and a meshing strategy are strongly interdependent. For example, the use of finite-difference methods is typically restricted to structured grids. Here again, the success of a simulation can depend on appropriate choices for the problem or class of problems of interest.

The most well-established and thoroughly validated general purpose CFD technique is the finite volume method. It is central to most of the commercially available CFD codes, for example: PHOENICS, FLUENT, FLOW3D and STAR-CD. These codes use the approach where unstructured meshes define the control volumes. This method consists of the following steps [16]:

- Integration of the governing equations of fluid flow over all the (finite) control volumes of the solution domain.
- Discretization involves the substitution of a variety of finite-difference-type approximations for the terms in the integrated equation presenting flow processes such as convection, diffusion and sources. This converts the integral equations into a system of algebraic equations.
- Solution of the algebraic equations by an iterative method.

2.2.4 ASSESSMENT AND INTERPRETATION OF RESULTS

Finally, the results of the simulation must be assessed and interpreted. This step can require post-processing of the data, for example calculation of forces and moments, and can be aided by sophisticated flow visualization tools and error estimation techniques. It is critical that the magnitude of both, numerical and physical-model errors are well understood.

2.3 USING FLUENT TO DO THE SIMULATION

FLUENT was the code used to do the simulations; it is a commercial CFD code. It has various applications in the aeronautical as well as chemical and thermo hydraulic industries. Various car manufacturers, commercial as well as Formula one, also use the code to perform aerodynamical design on their cars.

2.3.1 DESCRIPTION OF THE PROGRAM

FLUENT is written in the C computer language and makes full use of the flexibility and power offered by the language [17]. One of the major advantages of the program is that it has a separate pre-processing program attached for geometry modelling and mesh generation. The program (GAMBIT) is used to create the geometry and mesh the model before it is exported to FLUENT.

This is a very powerful method of performing analyses because modifications can easily be made to the geometry or mesh of a model without chancing anything to an analysis in FLUENT. GAMBIT uses an unstructured meshing strategy, thus reducing the set-up time when complex geometries are meshed.

2.3.2 VERIFICATION OF THE CODE

Since the PBMR is a nuclear power plant it has to be designed under strict rules and regulations. It has to comply with safety standards and quality assurance codes given by the National Nuclear Regulator (NNR) in order to obtain an operating licence in South Africa.

One regulatory requirement is that all applicable software codes used for the design of the PBMR must be verified and validated. It is a lengthy process to verify and validate these codes, especially CFD codes. In order to meet this requirement, PBMR has a dedicated section that is responsible for this task.

A report was written, containing information regarding the verification and validation of the CFD codes used in PBMR [18]. This report addresses the way that CFD codes handle and implement some of the basic aspects of fluid mechanics and heat transfer, ranging from the different heat transfer mechanisms and turbulence models to discretization schemes.

From this report it could be concluded that the performance of the codes was very similar, and one is not clearly superior to the other. FLUENT and Star CD are the CFD codes used for the design. Both the codes seem free from flaws in the way they simulate physical processes, and the solution algorithms are robust and sound.

3. SIMULATION MODEL

3.1 PREAMBLE

This chapter will elaborate in detail on how the model was incorporated in the code. The geometry and mesh are the first points to be addressed because simplifications in this area can reduce the required computation time significantly. However, it is also important to understand that these simplifications can dominate the simulation and provide unphysical results if wrongly implemented.

Operating, and boundary conditions are used to characterise the different characteristics of the real event. The right implementation of these conditions is also important to ensure that accurate answers are obtained. One of the major fields of discussion in this chapter will be to explain how the porous media model of FLUENT was used to simulate the capacitance.

Finally, all the specifications regarding the model have to be transformed into algebraic equations that give a mathematical description of the model. This transformation process is associated with certain options in order to simplify the equations. The discussion of these points will conclude this section.

3.2 SIMULATION SET-UP

3.2.1 DESCRIPTION OF THE MODEL

According to the ICS design report [19], approximately 20 ton steel wool will be placed inside a tank of approximately $100m^3$. The tank dimensions are in the order of 11.2m x ϕ3.75m and it is orientated vertically [20].

There are eight ICS storage tanks. The mentioned operating conditions refer to ICS tank no 1. This is the first tank that to fill when helium are extracted from the system. This tank was simulated, because it experiences the worst operating conditions. Worst operating conditions are defined in terms of the tank that operates at the highest system pressure.

Helium is introduced into the tank through a perforated tube, which has a 350mm diameter and 9500mm length. The tube is welded and supported on the centreline of the tank and perforated with 20mm holes on a pitch of 50mm over the last 6000mm of the pipe. The end of the pipe is closed. Refer to Figure 5 for an explanation of the geometry of the tank. The grey part of the pipe presents the perforated section. Figure 6 shows a close-up view of the front end of the perforated pipe.

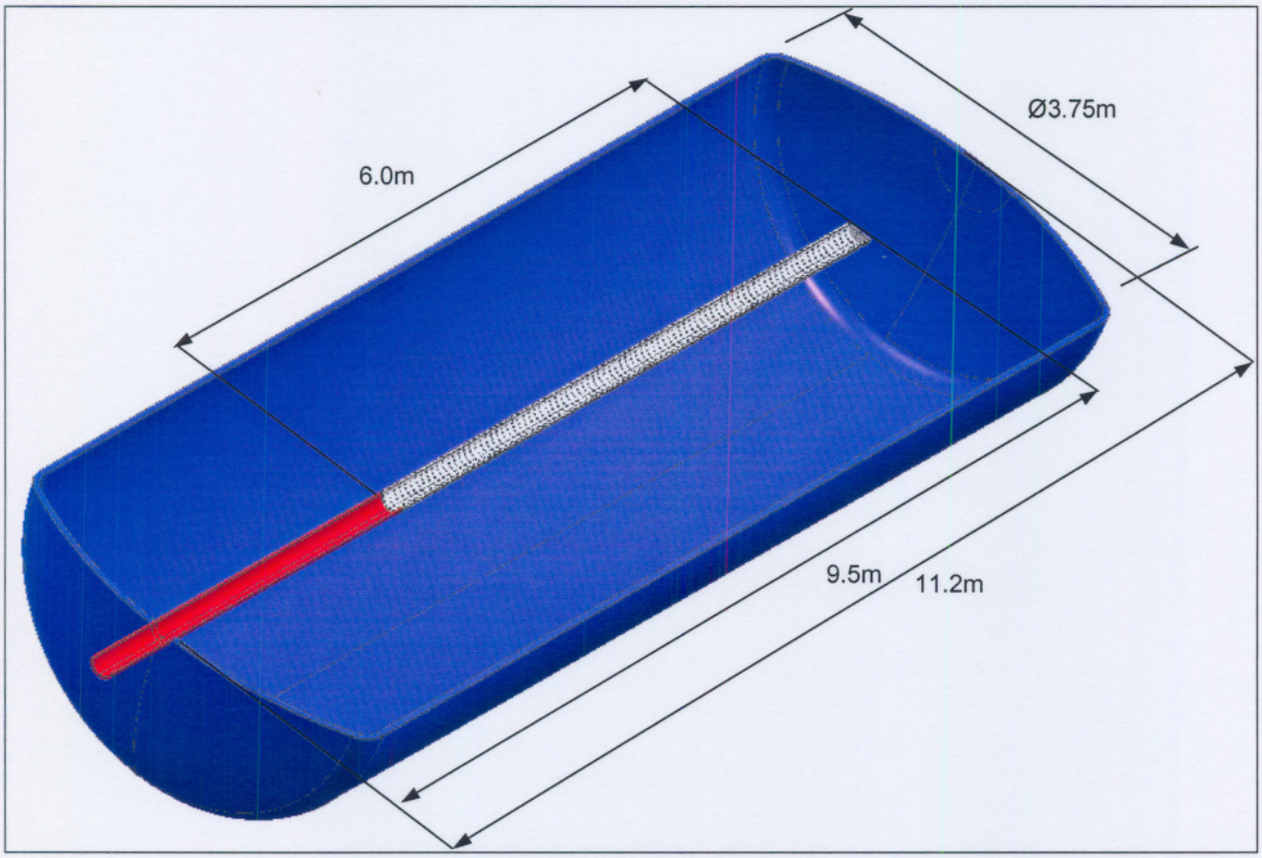

Figure 5: Geometry of ICS tank no 1.

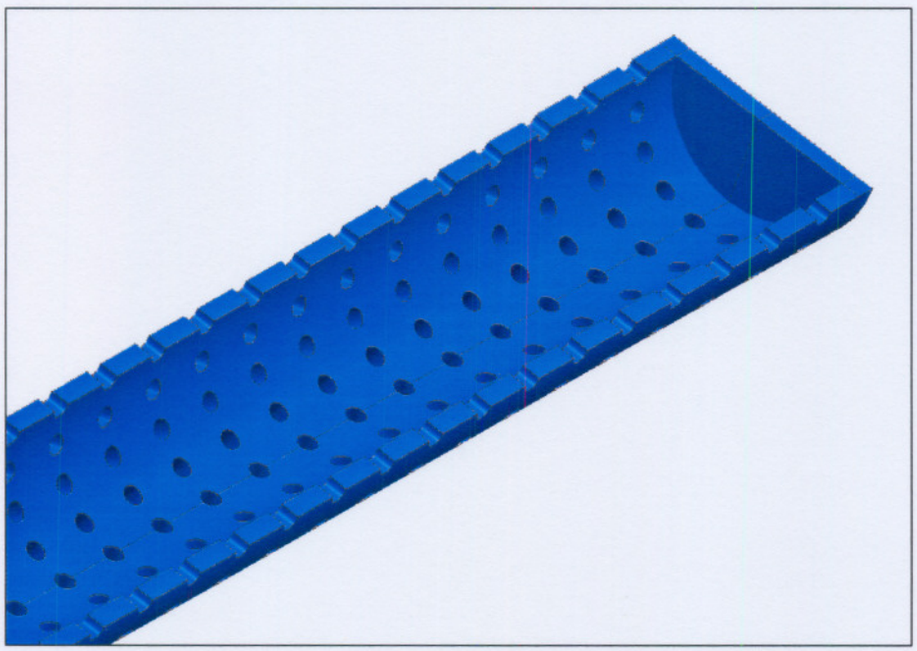

Figure 6: Front end of the perforated pipe

3.2.2 MODELLING ASSUMPTIONS

The helium and capacitance combination was modelled as a porous medium that was uniformly distributed throughout the whole tank. In order to model the flow within a porous medium, the pressure drop as a function of the fluid velocity in the medium should be supplied.

This correlation gives a mathematical representation of the resistance that the porous medium has against fluid flow. Literature shows that the pressure drop in a porous medium is highly dependent on the medium's porosity [9]. The porosity of a volume gives an indication of the volume fraction filled by solid material. A high porosity result a high-pressure loss through the medium; the tank-capacitance combination had a very low porosity (less than 5%).

No data could be found relating the pressure drop characteristics to the through flow velocity for a porous medium with comparable porosity to the simulated model. From the available literature [9] it appeared that the pressure loss for helium travelling through a porous medium (with a porosity of 95%) at velocities lower than 50m/s is almost insignificant (less than 1 MPa) when it is compared to mediums with high porosities (typically 50%). Refer to Figure 7.

For the purpose of a scoping study, it was unfeasible to determine this characteristic of the capacitance with an experimental process. Figure 7 indicates that the Pressure-Velocity correlation in a porous media is described with a parabolic curve. The graph in Figure 8 is an approximated correlation, but if this curve is extrapolated to 50m/s, a pressure drop of 51.50 kPa is obtained which seems acceptable according to the graph in Figure 7.

A sensitivity study was performed to assure that this assumption wouldn't dominate the results and that it still gives an accurate presentation of the physical event. This study will be discussed in more detail as part of the results.

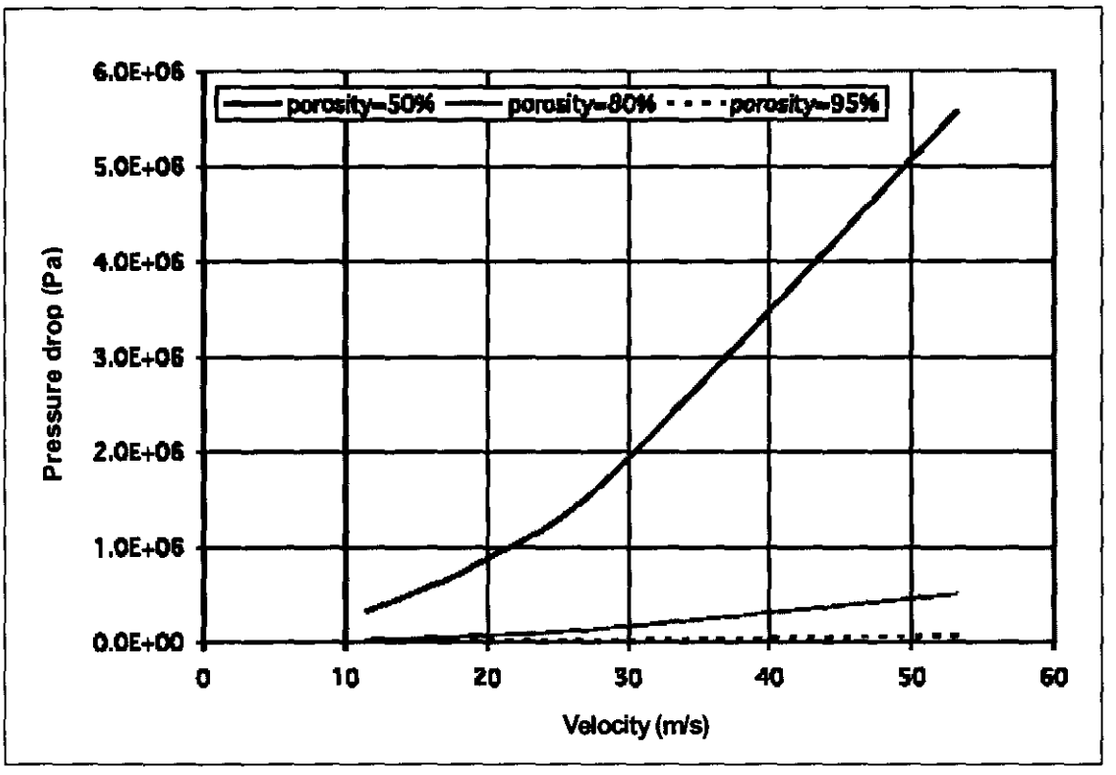

Figure 7: Pressure-Velocity correlation found in literature [9] for Helium in a porous media with different porosities.

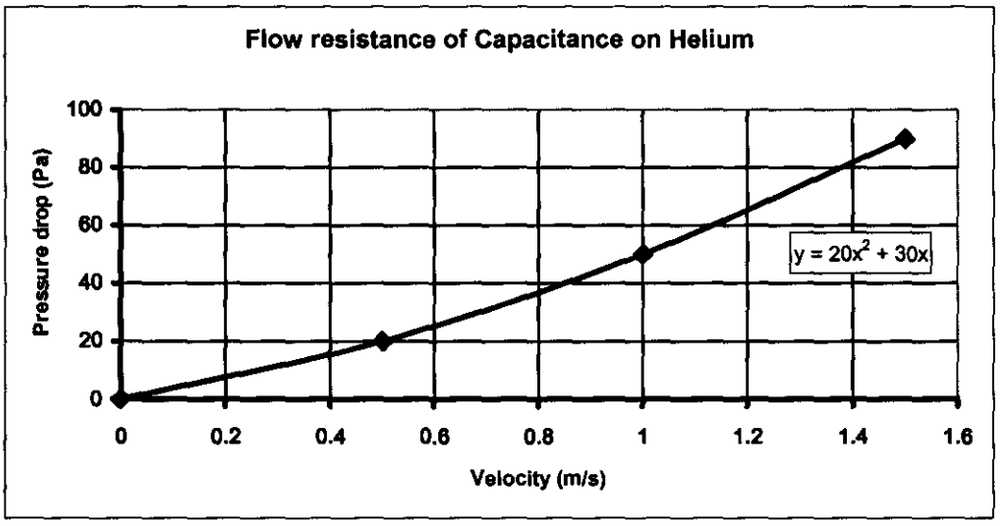

Figure 8: Approximated Pressure-Velocity correlation for Helium in capacitance.

3.2.3 MESH

Due to the symmetrical layout of the ICS tanks, it was possible to simulate it as a two dimensional axi-symmetric model. Modelling the holes in the perforated tube was addressed by simulating it as annuli. The total outflow area of the annuli was equal to the total outflow area of all the holes on the circumference of the tube. It was important that both the CFD and the physical model have the same outflow area.

The mesh of the model was refined in the areas where the flow behaviour was expected to be of great importance (area where the helium exits the perforated pipe). Figure 9 shows the mesh of the final model; the helium as well as the capacitance is coloured in green, while the steel parts is coloured in black. The cell refinement close to the perforated pipe can be noted. The geometry of the simulated model was orientated horizontally for axi-symmetric modelling purposes only.

Large variations in cell sizes can lead to numerical errors when performing a CFD analysis. If this occurrence is present in a model, it is necessary to do a grid sensitivity study to ensure that the solution is grid-independent. Figure 9 indicates that there are large differences in the cell sizes of the mesh.

However, this was only a scoping study to evaluate the concept and the absolute values weren't used for detail design purposes. A grid sensitivity study can influence the results, but not in a way that it will have a negative impact on the validity of the scoping study.

Nevertheless, before these results can be used for a detail design study, grid sensitivity studies must be done on at least one of the cases to determine the impact on the absolute values of the results.

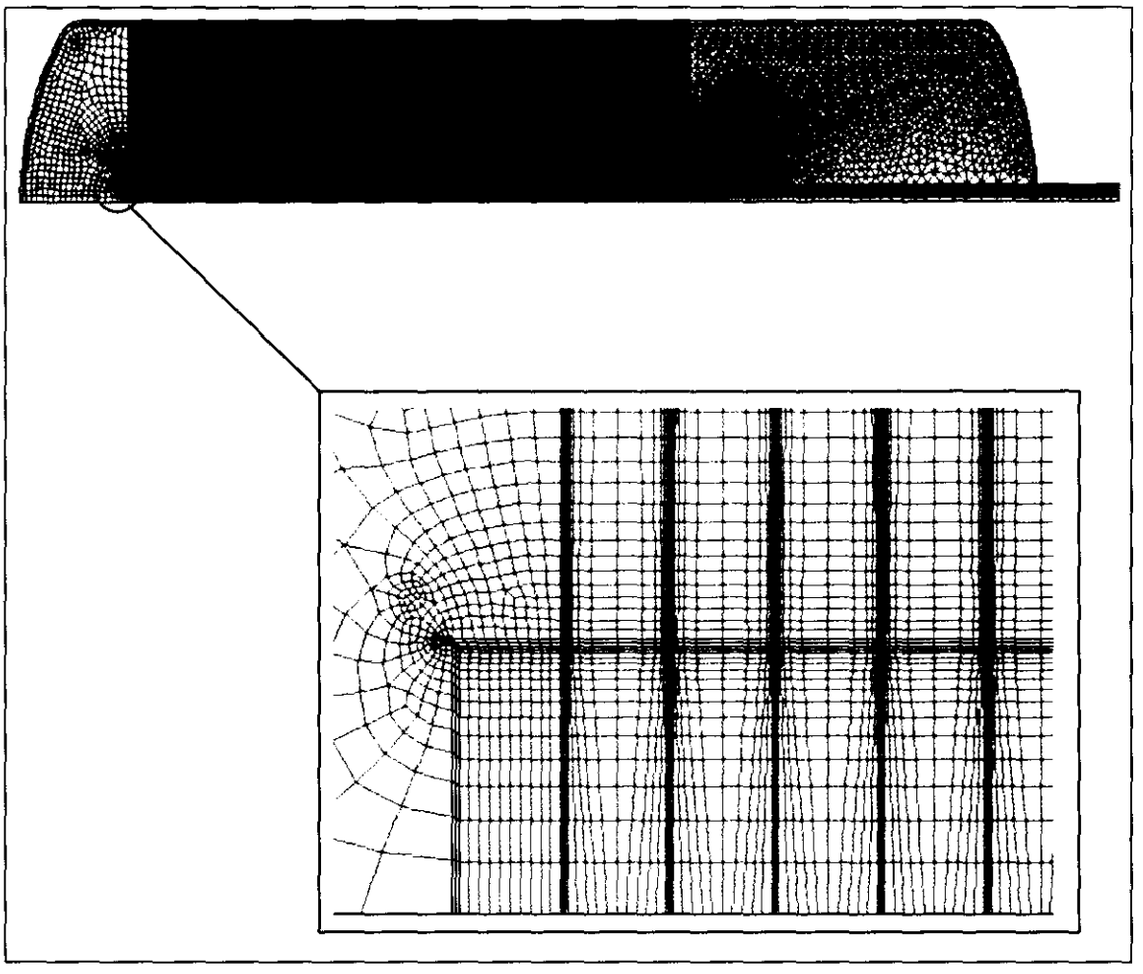

Figure 9: The mesh of the model.

3.2.4 MATERIAL PROPERTIES

PBMR has a database that contains the thermo physical properties of all the materials used in the PBMR design [21]. These properties are validated against various sources to ensure that it gives an accurate mathematical presentation of the actual behaviour of the materials. Helium as well as steel was characterized according the corresponding properties in the database.

3.2.5 OPERATING CONDITIONS

The injection of Helium into the system had to be modelled as a transient state condition. A period of 60 seconds was modelled at a time step size of 0.01 second. The operating pressure at which the simulation was done was specified as 3019 kPa. This means that the initial gauge pressure in the tank, before the injection process started, was 0 kPa. The effect of gravity was neglected in the simulation.

3.2.6 BOUNDARY CONDITIONS

Table 1 gives the implemented boundary types and the values at the appropriate locations in the model. It was decided to use a mass flow boundary at the tank's inlet, where a constant mass flow rate is specified at a certain temperature.

The temperature applied to the tank outer wall corresponds to the temperature mentioned in the development specification [7]. This temperature on the tank outer wall is maintained by the HVAC system, which cools the storage area where the tanks are situated. The axis boundary type was used to present the centreline of an axi-symmetric geometry

The capacitance, as presented by the cell zone in the tank, was characterised according to the porous media model of FLUENT. The code determines the pressure loss in the flow via user inputs; using the values as supplied in Figure 8. Heat transfer through the medium can also be represented, subject to the assumption of thermal equilibrium between the medium and the fluid flow [17].

The porous media model incorporates an empirically determined flow resistance in a region of the model defined as "porous". In essence, the porous media model is nothing more than an added momentum sink in the governing momentum equations. This momentum sink contributes to the pressure gradient in the porous cell, creating a pressure drop that is proportional to the fluid velocity in this region [17].

Table 1: Summary of the boundary types that were used for the simulations

Locations	Boundary type	Value
Inlet of tank	Mass flow inlet	m = 9.0 *kg/s* T = 393.15 *Kelvin*
Tank wall	Wall	T = 293.15 *Kelvin*
Symmetry axis	Axis	---
Capacitance	Porous media	Viscous resistance = 1246883.0 $1/m^2$ Inertial resistance = 11.001 *1/m* Porosity = 0.975

The equation shown below presents the added momentum source/sink term that is used to model the porous media. The equation consists of two parts: a viscous loss term (the first term on the right-hand side), and an inertial loss term (the second term on the right-hand side). The coefficients (C1 and C2) of these viscous and inertial losses need to be specified in order to characterize the porous media. This is the resistances referred to in Table 1.

$$\nabla P = \frac{\mu}{\alpha}.V + \Phi.\tfrac{1}{2}\rho.V^2$$

$$\nabla P = \frac{\Delta P}{L} \quad \text{(Pressure gradient)}$$

$$C1 = \frac{1}{\alpha} \quad \text{(Viscous resistance)}$$

$$C2 = \Phi \quad \text{(Inertial resistance)}$$

The pressure-velocity correlation shown in Figure 8 is represented by the equation shown below. When this equation is substituted into the momentum source term for the porous media the required inputs for the simulation can be calculated for a specific unit length in the porous media. It is normally necessary to specify the resistance values for the different flow directions in the porous media, but in this instance it was assumed that the steel wool have an equal packing, resulting in equal resistances in both, the x as well as the y directions.

$$\Delta P = 20.V^2 + 30.V$$

$$30 = \frac{\mu}{\alpha}$$

$$20 = \Phi\tfrac{1}{2}\rho.$$

The fluid properties used to calculate the resistances correspond to the initial conditions in the tank. If the values are substituted into the mentioned equations, the viscous as well as inertial resistances can be calculated.

$\mu = 2.434.10^{-5}$ kg/m.s
$\rho = 3.636$ kg/m^3

$C1 = 1246882.793$ 1/m^2 (Viscous resistance)
$C2 = 11.001$ 1/m (Inertial resistance)

FLUENT solves the standard energy transport equation in porous media regions with modifications to the conduction flux and the transient terms only. In the porous medium, the conduction flux uses an effective conductivity and the transient term includes the thermal inertia of the solid region on the medium. These values are calculated with the porosity of the porous medium. This approach is commonly used in industry and correlates well to experimental data [22].

As mentioned before, the porosity of the medium is specified in terms of the volume fraction of solid material in the medium. The calculation shows that the capacitance has a porosity of 0.975.

$$\text{Porosity} = \frac{\text{Volume of fluid}}{\text{Total volume}}$$

Total volume = Tank volume = ±100m^3

Mass of Porous medium = 20 000kg

Density of porous medium = 7850kg/m^3

$$\text{Volume of porous medium} = \frac{20000}{7850}$$
$$= 2.548\text{m}^3$$

$$\text{Porosity} = \frac{(100 - 2.548)}{100} = 0.975$$

3.3 SOLVER FORMULATION

3.3.1 SOLVING APPROACH

The solving approach determines how the continuity, momentum, energy and species (not applicable) equations will be solved. The equations could either be solved sequentially (segregated) or simultaneously (coupled). For the application of this project the default approach of FLUENT, the segregated approach, was chosen.

3.3.2 TURBULENCE MODELLING

For normal pipe flow, the transition from laminar to turbulent flow occurs at a Reynolds number of approximately 2300 [23]. The calculated Reynolds number in the inlet pipe ranges from $1{,}345.10^6$ at the pipe inlet to $1{,}711.10^4$ at a perforated hole (Refer to Appendix A.1). Form these numbers; it is evident that the flow in the pipe was turbulent.

There was some uncertainty in calculating the Reynolds number in the porous medium because of all the unknown parameters. From a literature survey on turbulence modelling in porous media it appeared that turbulence already start showing at Reynolds numbers of 60 [24]. The transition from laminar to turbulent in porous flow field takes place at a Reynolds number of 100.

From this source of information, it was decided to simulate the flow in the model as turbulent and a turbulent flow model had to be chosen. The simplest of the "complete models" of turbulence are two-equation models in which the solution of two separate transport equations allows the turbulent velocity and length scales to be independently determined [25].

The standard k-ε model in FLUENT falls within this class of turbulence models and was used. This model is robust and reasonably accurate for a wide range of turbulent flows. It is a semi-empirical model, and the derivation of the model equations relies on phenomenological considerations and empiricism.

3.3.3 DISCRETIZATION

When the flow is aligned with the grid (e.g., flow in a rectangular duct modelled with a quadrilateral or hexahedral grid) the first-order upwind discretization may be acceptable. When the flow is not aligned with the grid (i.e., when it crosses the grid lines obliquely), however, first-order convective discretization increases the numerical discretization error (false diffusion) [26].

For triangular and tetrahedral grids, since the flow is never aligned with the grid, you will generally obtain more accurate results by using second-order discretization schemes. For quadrilateral and hexahedral grids, you will also obtain better results using a second-order discretization scheme, especially for complex flows.

Although the mesh consisted only of quadrilateral elements, the flow was turbulent and not always aligned with the grid. However, second-order discretization schemes need more computing power in solving a flow flied than first-order schemes and it increases the simulation time significantly.

Since this was only a scoping study to evaluate the concept, the first-order discretization scheme was used. Again, the credibility of the study won't be influenced by this inaccuracy in the simulation as long as the values won't be used for detail design purposes.

4. INTERPRETATION AND VERIFICATION OF RESULTS

4.1 PREAMBLE

This chapter will discuss how the simulation results were interpreted and verified. The first objective was to determine if the concept made an improvement in the attempt to reduce the necessary tank storage area.

The most effective way to evaluate the success of the proposal was to compare the total pressure inside the tank (with capacitance) after the specified injection period with the case where no capacitance was simulated in the tank. A lower pressure inside the tank would mean that more helium can be stored inside the tank before the maximum tank operating pressure is reached. The model with no capacitance in the tank will be referred to as the reference case.

The success of this concept is based on the large heat transfer area available when heat has to be transferred from the helium to capacitance. To optimally use the advantage, a few injection concepts were evaluated to find the method that maximises the helium exposure to the capacitance.

The last section of the chapter will discuss the verification of the results. Firstly, a sensitivity study was used to quantify the influence of a change in the resistance values (of the porous medium) on the results. The second part contains the mass and energy conservation checks performed on each simulation to ensure that the solutions were converged.

4.2 COMPARISON BETWEEN PROPOSED CONCEPT WITH REFERENCE CASE

It was important to have data available on the model with no capacitance in the tank; this data can be used to quantify the improvement caused by the capacitance above the reference case. A model without any porous media was simulated in order to obtain this data.

Table 2 show the comparison in total pressures between the reference case and the tank filled with capacitance. It appeared the capacitance made a significant improvement in terms of the total pressure in the tank after the injection period. The use of capacitance almost decreased the total pressure inside the tank by 2300 kPa, which gives an improvement of about 24%.

Table 2: Comparison between the reference case and the tank filled with capacitance.

Model	Total Pressure (kPa)
Tank without capacitance (Reference case)	9426.13
Tank filled with capacitance	7148.08

In Figure 10 a comparison between the temperature distributions of helium in the tank for the different cases is shown. The upper picture presents the tank without capacitance, while the lower picture present the tank filled with capacitance. It is visible that the average helium temperature is much lower in the tank with capacitance than the tank without capacitance.

Unfortunately, the capacitance causes a high temperature concentration at the furthest end of the pipe. This is caused by a stagnation region existing at the end of the pipe, forcing most of the Helium to exit through the holes in the vicinity of the stagnation region. The analysis shows that the perforated pipe does not distribute the Helium equally throughout the tank.

This scenario indicated that there is still room for improvement regarding the high heat transfer area that the capacitance provides. The next section will evaluate a few possible concepts of injecting helium into the tank to optimally use the capacitance.

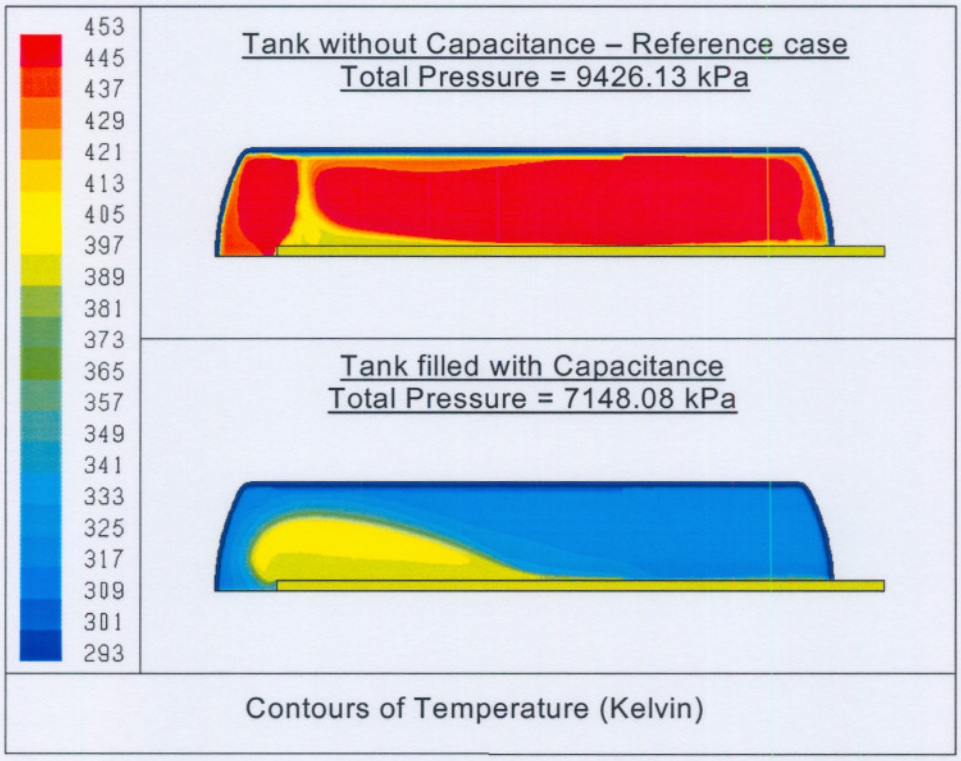

Figure 10: Temperature distribution of the helium in the tanks after a 60-second injection period.

4.3 OTHER INJECTION CONCEPTS EVALUATED

In chapter 1 it was explained that the large surface-to-volume ratio of this concept results in a system with a quick thermal response. Exposing more helium to the capacitance would increase this response and result in a lower final total pressure.

This section discusses a concept study to introduce helium into the tank to get optimal exposure to the capacitance. Each concept was evaluated on the basis of the total pressure in the tank after the 60-second injection period.

The first concept had no pipe in the tank at all (Figure 11). The purpose of this simulation was to establish if the perforated pipe had any positive influence on the concept. From the results it appeared that the pipe compliments the function of the design, although it is a very small contribution; the pressure in the tank increased to 7148.50 kPa (Figure 12).

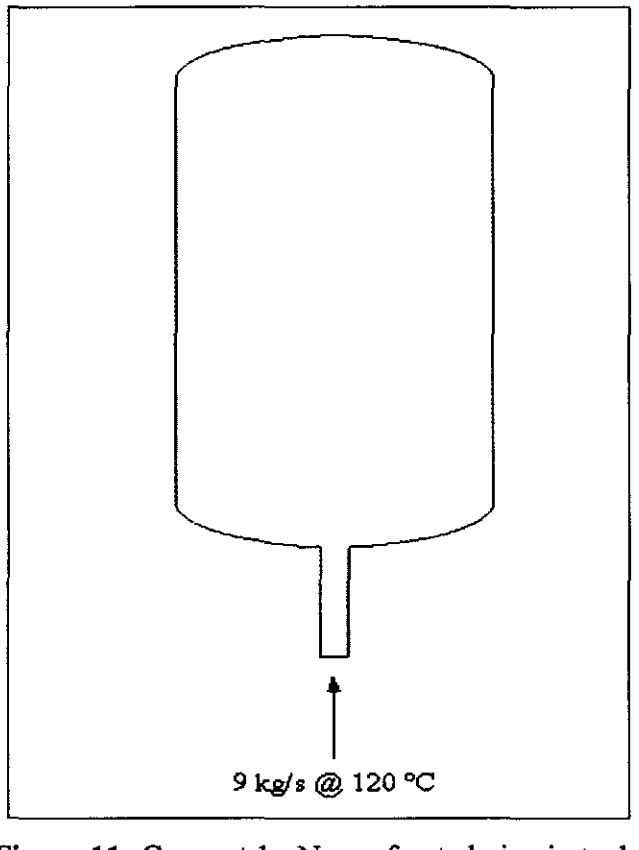

Figure 11: Concept 1 - No perforated pipe in tank

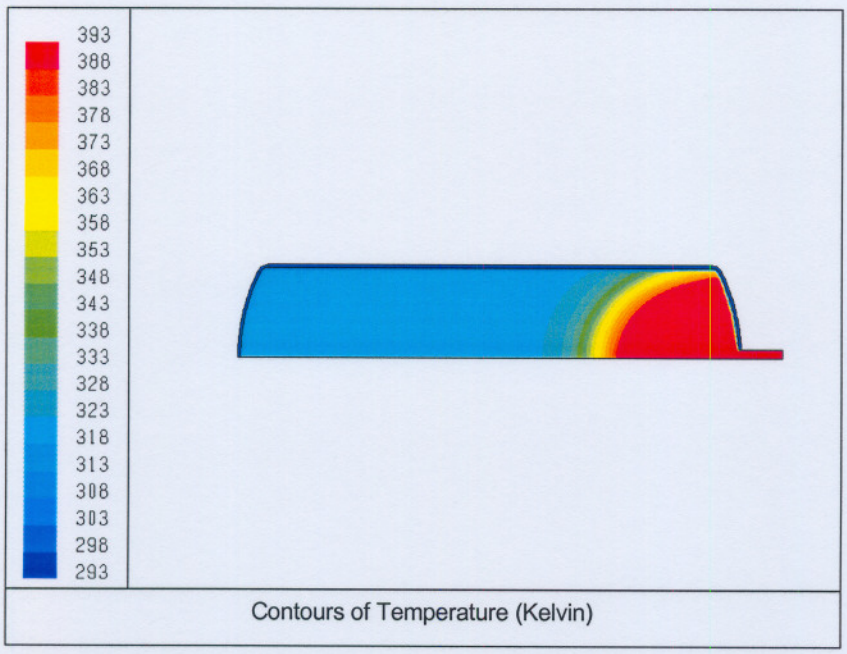

Figure 12: Concept 1 - Injection of Helium into tank, with capacitance and no perforated pipe. Total pressure inside tank = 7148.50 kPa.

The second concept used a perforated pipe with varying diameter. The pipe diameter was decreased towards the end using 3 different standard pipe diameters of 450mm, 350mm and 250mm, respectively (Figure 13).

This increased the flow resistance and forced the helium out of the pipe earlier. The outflow area near the tank entrance was larger because more holes can be located on the circumference of a pipe with a larger diameter and it allowed more flow to exit the pipe in this region.

The temperature contours in Figure 14 show that the helium is distributed uniformly through the tank. Considering the total pressure inside the tank (7135.20 kPa), this concept made an improvement to the standard perforated pipe but there were still high temperature regions occurring in the capacitance.

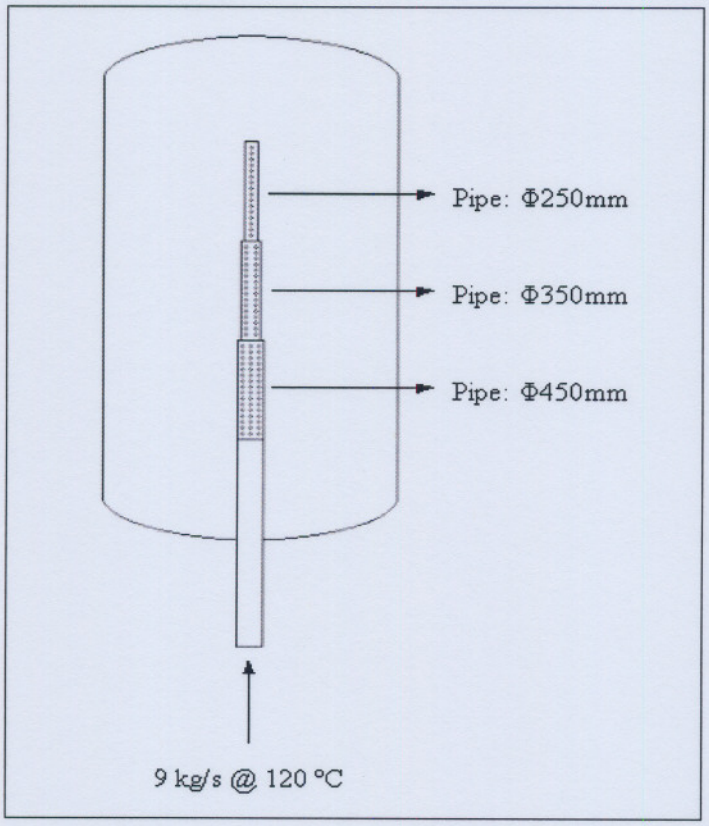

Figure 13: Concept 2 – Perforated pipe consisting of 3 different pipe diameters

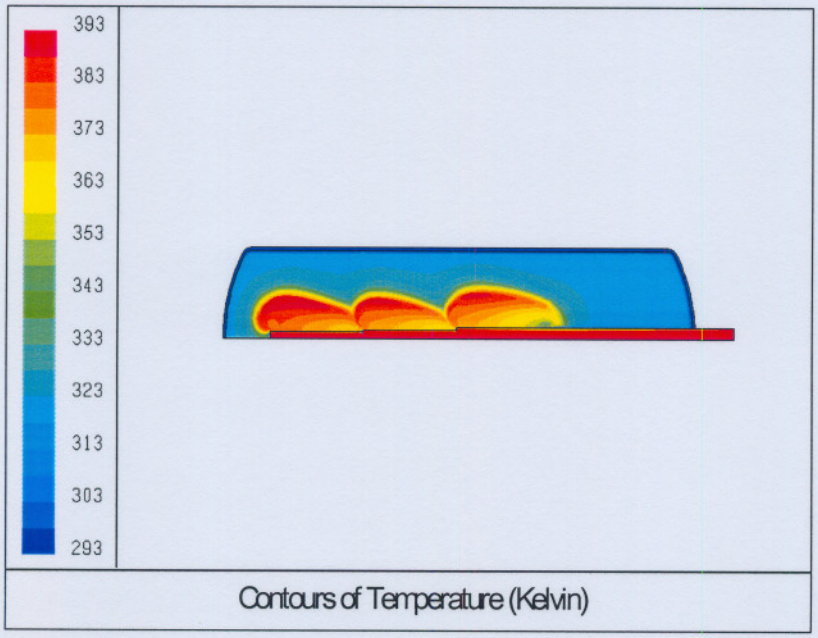

Figure 14: Concept 2 - Injection of Helium into tank, with capacitance and varying pipe diameter. Total pressure = 7135.20 kPa.

The third concept evaluated, increased the outflow area towards the entrance of the tank by increasing the diameter of the perforated holes (Figure 15). Holes with diameters of 24mm, 28mm and 30mm were used, respectively.

This concept resulted in the lowest total pressure inside the tank (7123.50 kPa) and the temperature distribution through the tank is also reasonably uniform (Figure 16). There is still some room for improvement on this concept, but it illustrated that this concept is the best way of decreasing the total pressure inside the tank with the least impact on cost and manufacturability.

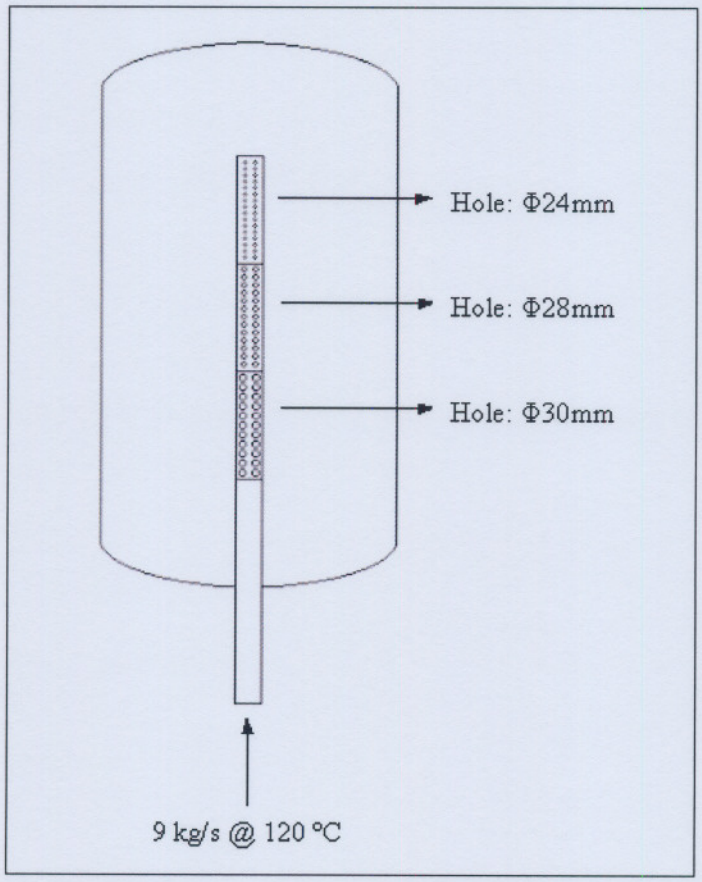

Figure 15: Concept 3 – Perforated holes consisting out of 3 different diameters

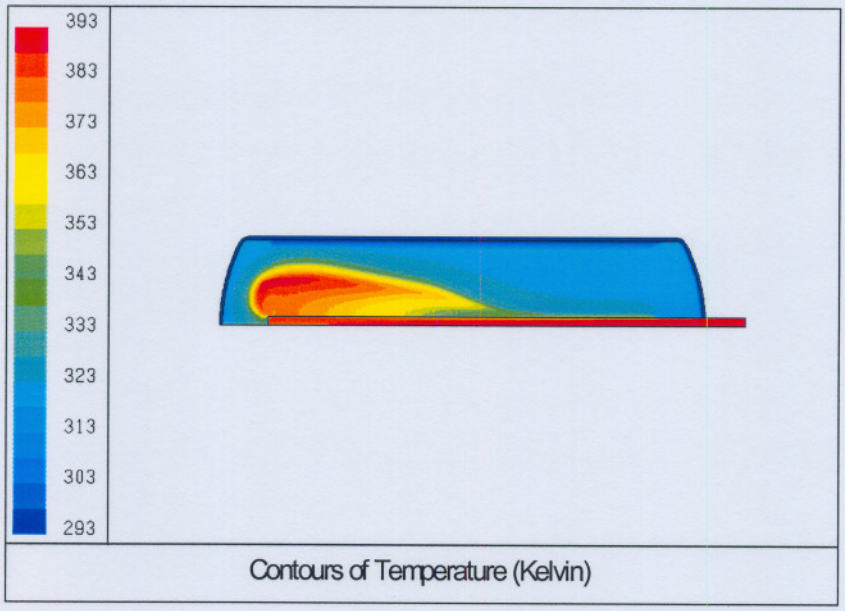

Figure 16: Concept 3 - Injection of Helium into tank, with capacitance and pipe with varying hole diameter. Total pressure inside tank = 7123.50 kPa.

Table 3 gives a summary of all the analyses performed. The total pressure inside the tank can be compared for each case to measure the improvement caused by the capacitance on the efficiency of the system. The table also show that the efficiency can further be improved by obtaining a uniform temperature distribution in the tank. An improvement of about 24.5% is obtained when the tank without capacitance (reference case) is compared to the most optimal concept.

Table 3: Total pressures in tank for the different injection concepts.

Configuration	Total pressure inside the tank (kPa)
Tank without capacitance – reference case	9426.13
Tank with capacitance	7148.08
Concept 1 – No pipe in tank	7148.50
Concept 2 – Perforated pipe with 3 different pipe diameters	7135.20
Concept 3 – Perforated pipe with 3 different hole diameters	7123.50

4.4 VERIFICATION OF RESULTS

4.4.1 SENSITIVITY STUDIES ON THE POROUS MEDIUM

As discussed previously, no literature could be found in connection with the pressure loss occurring when a porous medium with low porosity is used as an obstruction in a flowfield. The CFD code needs this information in order to characterise the porous medium. A pressure-velocity correlation based on assumptions was used to do this characterization.

The influence of the assumption-based correlation on the results had to be quantified. The sensitivity of a change in the resistance values of the porous medium (inertial as well as viscous) on the results was evaluated; it was done by increasing and decreasing the calculated values by 10%. The values weren't changed by more than 10% because of the possibility that it can influence the distribution of gas in the tank and subsequently result in an invalid comparison.

The simulations were performed on the model with the standard perforated pipe and the average tank pressures were compared. The results of this study are shown in Table 4. The maximum deviance in the end results is 0.05%. Although there were small differences in the end tank pressures, this study showed that a small inaccuracy in resistance values of the porous medium wouldn't dominate the final results. From this study it was concluded that the values used to characterize the porous media was acceptable for scoping study purpose.

Table 4: Results of sensitivity study performed on the porous medium

Configuration	Total Pressure inside (kPa)
Original values	7148.08
Original values + 10%	7148.42
Original values - 10%	7145.22

4.4.2 CONSERVATION CHECKS

It was of great importance to confirm that the obtained results were an accurate representation of the real event. The most sensible way to verify the results was by doing conservation checks to ensure that each simulation solution has converged. Mass and energy balances were done to substantiate the conservation checks.

The first law of thermodynamics was used for the energy balance on the models. Since gas is pumped into a tank at a constant mass flow rate, the uniform-state-uniform-flow process approach was used to calculate the balance [27]. The equation describing this specific process is discussed below. Note that the control volume was chosen around the tank.

$$Q_{cv} + \sum m_i \left(h_i + \frac{V_i^2}{2} \right) = m_2 u_2 - m_1 u_1$$

Q_{cv} = Heat tansfer over tank walls (J)
m_i = Mass injected to tank (kg)
h_i = Enthalpy of injected mass (J/kg)
V_i = Velocity of injected mass (m/s)
m_1 = Initial mass in tank (kg)
m_2 = Mass in tank after injection period (kg)
u_1 = Initial internal energy in tank (J/kg)
u_2 = Inernal energy in tank after injection period (J/kg)

Enthalpy was calculated according to the PRMR thermo physical properties [21]. It was calculated with the corresponding temperature and pressure of the gas in the region of interest. The formulation of this equation is shown below.

$$H = 5195(T - 273.16) + \frac{1108.27}{T^{0.2}}\left(10^{-5}.P - 1\right)$$

T = Temperaure(Kelvin)
P = Pressure(Pa)

The mass conservation balance consists of comparing the mass of helium in the tank after the injection period to the initial mass of helium in the tank plus the injected amount of gas. The equation describing this conservation balance is shown below.

$$m_i + \dot{m}.t = m_e$$

$$m_i = \rho_{ti}.V_t + \rho_{pi}.V_p$$
$$m_e = \rho_{te}.V_t + \rho_{pe}.V_p$$

m_i = Initial mass of helium in tank (kg)
$\dot{m}$ = Injection mass flow rate (kg/s)
t = Injection period (sec)
m_e = Mass of helium in tank after injection period (kg)
V_t = Volume of helium in tank (m^3)
V_p = Volume of helium in perforated pipe (m^3)
ρ_{ti} = Initial helium density in tank (kg/m^3)
ρ_{pi} = Initial helium density in perforated pipe (kg/m^3)
ρ_{te} = Helium density in tank after injection period (kg/m^3)
ρ_{pe} = Helium density in perporated pipe after injection period (kg/m^3)

Table 5 show the results of the accomplished conservation balances. The two yellow columns present percentage deviance in the constructed balance for each case. These deviances are caused by averaging errors that occur due to fluctuations in the flowfield when post-processing was done. Other possible reasons can be the existence of round off errors in the numerical solver as well as the specification of the convergence criteria.

However, the conservation checks showed that the results obtained from the simulations could be trusted for the purpose of this evaluation study. The detailed calculations of the checks can be found in Appendix A.2.

Table 5: Summary of the conservation checks for each simulation

Model	Mass Conservation			Energy Conservation		
	$m_i + \dot{m}.t$	m_e	Deviance	$Q_{cv} + \sum m_i\left(h_i + \frac{V_i^2}{2}\right)$	$m_2u_2 - m_1u_1$	Deviance
	kg	kg	%	kJ	kJ	%
Reference case (No Capacitance)	1055.56	1052.17	0.32	345669.93	348414.06	0.79
Capacitance	1042.79	1048.03	0.50	344434.91	343709.95	0.21
Concept1: No pipe	1042.95	1048.36	0.52	344390.79	342971.51	0.41
Concept2: 3 Pipes	1043.04	1041.13	0.18	344401.73	343166.30	0.36
Concept3: 3 Holes	1042.82	1046.60	0.36	344442.11	342776.86	0.48
Sensitivity: +10%	1042.79	1048.05	0.50	344441.99	342863.12	0.46
Sensitivity: -10%	1042.79	1047.61	0.46	344438.26	343429.93	0.29

5. CONCLUSION AND RECOMMENDATIONS

The major objective of this study was to determine the feasibility of using capacitance in the ICS tanks of the PBMR. It was found that the capacitance made a significant improvement in reducing the total pressure in the tanks. The implementation of this concept made an improvement of about 24% by reducing the total pressure from 9426.13 kPa to 7148.08 kPa.

For this reason, smaller tanks can be used to store the same amount of helium, or alternatively, more helium can be stored in the same tank, before reaching the tank's maximum operating pressure. The capacitance provides a large heat transfer area, resulting in a system with a quick thermal response when absorbing the energy contained in the injected gas.

The advantage the capacitance provides, was further optimised by distributing the injected helium more evenly throughout the tank. This was accomplished by varying the diameter of the perforated holes. This modification should have a minimal impact on manufacturing costs and results in an additional reduction of the total pressure to 7123.50 kPa. This is a further improvement of about 0.5% to the standard perforated pipe.

It is recommended that this concept first be optimised to find the optimal distribution of helium in the tank before implementation in the actual design. Since this was a scoping study, the data can't be used to make detail design changes to the tanks. It is advised that the actual pressure-velocity relationship of the capacitance be determined and used to quantify the impact on the results.

Another recommendation is to perform a sensitivity study of the mass of capacitance in the tank on the results. A larger capacitance mass in the tank can increase the heat transfer area in the tank to a certain extent and absorb more energy from the helium. However, it will decrease the porosity and cause a larger pressure loss through the capacitance. This suggestion needs to be tested before any conclusions can be made in this regard.

Similar systems in industry sometimes isolate the capacitance from the tank's wall [28]. This implies that there is no direct contact between the capacitance in the tank wall. The major advantage of this modification is that the heat transfer between the capacitance and the tank wall is reduced. Consequently, the temperature on the outer walls of the tank will be lower and it will reduce the heat load on the HVAC system. A simulation can be done to quantify the improvement.

6. REFERENCES

[1] Pebble Bed Modular Reactor Brochure, PBMR (Pty) Ltd, 2003

[2] Pebble Power, *Popular mechanics* 1 no.2 (2002) 78-81

[3] Koster, A, Matzner, H.D, Nicholsi, D.R, PBMR design for the future, *Nuclear and Design* 222 (2003) 231-245

[4] Internet Web Site of the company PBMR, www.pbmr.co.za, 2002

[5] Modular Milestone, *Popular Mechanics* 1 no.7 (2002) 85

[6] Introduction to the Pebble Bed Modular Reactor, 009949-185, PBMR Document and Data Control Centre, South Africa, 2003

[7] Inventory Control System (ICS) Development Specification, ICS-000000-62, PBMR Document and Data Control Centre, South Africa, 2003

[8] Mills, A.F, Basic Heat and Mass Transfer, Richard D Irwin Inc, 1995

[9] Raffray, A.R, Pulsifer, J.E, MERLOT: a model for flow and heat transfer through porous media for high flux applications, *Fusion engineering and design* 65 (2003) 57-76

[10] Amiri, A, Vafai, K, Transient analysis of compressible flow through a packed bed, *International Journal of Heat and Mass Transfer* 41 (1998) 4259-4279

[11] Sanderson, T.M, Cunningham, G.T, Performance and efficient design of packed bed thermal storage systems. Part 1, *Applied Energy* 50 (1995) 199-132

[12] Ichimiya, K, Matsuda, T, Kawai, Y, Effects of a porous medium on local heat transfer and fluid flow in a forced convection field. *International Journal of Heat and Mass Transfer* 40 (1997) 1567-1576

[13] Kheder, C.B, Cherif, B, Sifaoui, M.S, Numerical study of transient heat transfer in semitransparent porous medium, *Renewable Energy* 27 (2002) 543-560

[14] Rousseau, P.G, Advanced Thermal-Fluid Systems Course Notes, School of Mechanical and Materials Engineering, PU for CHE, 2002

[15] Lomax, H., Pulliam, T.H., Zingg, D.W., Fundamentals of Computational Fluid Dynamics, NASA Research Centre and University of Toronto Institute for Aerospace Studies, 1999.

[16] Versteeg, H.K, Malalasekera, W, An Introduction to Computational Fluid Dynamics – The Finite Volume method, Longman, 1995

[17] Fluent Inc. Product Documentation: FLUENT 6.1

[18] CFD Software Validation Report, PP260-016021-3713, PBMR Document and Data Control Centre, South Africa, 2003

[19] Inventory Control System (ICS) Design Report, ICS-000000-37, PBMR Document and Data Control Centre, South Africa, 2003

[20] Technical drawing, Part No: 002676 Rev 1, PBMR Document and Data Control Centre, South Africa, 2003

[21] PBMR Thermo physical Properties, 003392, PBMR Document and Data Control Centre, South Africa, 2003

[22] Zhang, H.Y, Huang, X.Y, Heat transfer studies in a porous heat sink characterized by circular ducts, *International Journal of Heat and Mass Transfer* 44 (2001) 1593-1603

[23] White, F.M, Fluid Mechanics – 4th ed, McGraw-Hill, 1999

[24] Logtenberg, S.A, Dixon, A.G, Computational fluid dynamics studies of fixed bed heat transfer, *Chemical Engineering and Processing* 37 (1998) 7-21

[25] Ferziger, J.H, Perić, M, Computational Methods for Fluid Dynamics – 3rd ed, Springer, 2002

[26] Patankar, S.V, Numerical Heat Transfer and Fluid Flow, Hemisphere Publishing Corporation, 1980

[27] Sontag, R.E, Brognakke, C, Van Wylen, G.J, Fundamentals of Thermodynamics –5th ed, John Wiley & Sons, 1998

[28] Bejan, A, Thermodynamic optimisation of geometry in engineering flow systems, *Extergy an International Journal* 1(4) (2001) 269-277

A. APPENDICES

A.1 REYNOLDS NUMBER CALCULATIONS

Reynolds number at Inlet of Pipe :

$$A = \pi.\frac{D^2}{4}$$

A = Cross sectional area of pipe

D = 0.35 m (Internal diameter of pip)

$A = 0.0962 \ m^2$

$m_t = 9$ kg/s (Total mass flow rate)

$$Re = \frac{m_t.D}{A.\mu}$$

$\mu = 2.434.10^{-5}$ kg/m.s

Re = 1345129

∴ The flow is turbulent

Reynolds number at Perforated hole :

$$A = \pi.\frac{D^2}{4}$$

A = Area of perforated hole

D = 0.02 m (Diameter of perforated hole)

$A = 0.0003142 \ m^2$

$m_t = 9$ kg/s (Total mass flow rate)

n = 1376 (Number of perforated holes)

$$m = \frac{m_t}{n}$$

m = 0.006541 kg/s

$$Re = \frac{m.D}{A.\mu}$$

$\mu = 2.434.10^{-5}$ kg/m.s

Re = 17110

∴ The flow is turbulent

A.2 CONSERVATION CHECKS

Model: No Capacitance (Reference Case)

Time step	Time seconds	Temperature K	Gauge Pressure Pa	Abs Pressure Pa	Density kg/m^3	Heat transfer Watt	Velcoity m/s	Enthalpy J/kg
0	0.00	392.75	0	3019000	3.872	0.0	24.777	631066.22
500	5.00	392.75	527945	3546945	4.350	-99.0	22.054	632838.01
1000	10.00	392.75	1059715	4078715	5.002	-692.0	19.182	634622.63
1500	15.00	392.75	1591713	4610713	5.653	-2080.7	16.971	636408.02
2000	20.00	392.75	2125777	5144777	6.307	-4406.9	15.211	638200.34
2500	25.00	392.75	2660298	5679298	6.962	-7717.7	13.780	639994.19
3000	30.00	392.75	3196539	6215539	7.619	-12037.6	12.592	641793.82
3500	35.00	392.75	3733357	6752357	8.277	-17344.5	11.591	643595.38
4000	40.00	392.75	4270653	7289653	8.935	-23604.7	10.737	645398.55
4500	45.00	392.75	4808525	7827525	9.595	-30770.0	9.999	647203.65
5000	50.00	392.75	5347060	8366060	10.255	-38773.6	9.356	649010.97
5500	55.00	392.75	5886102	8905102	10.915	-47550.0	8.790	650820.00
6000	60.00	392.75	6407191	9426191	11.554	-57047.2	8.304	652568.77

Model: No Capacitance (Reference Case)

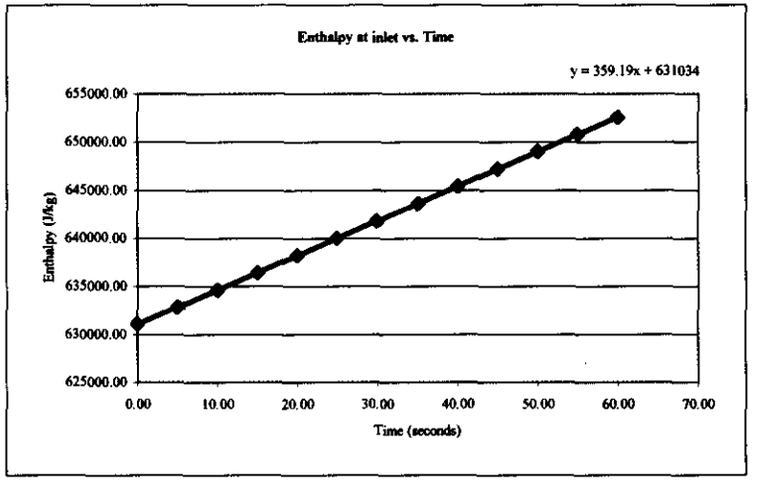

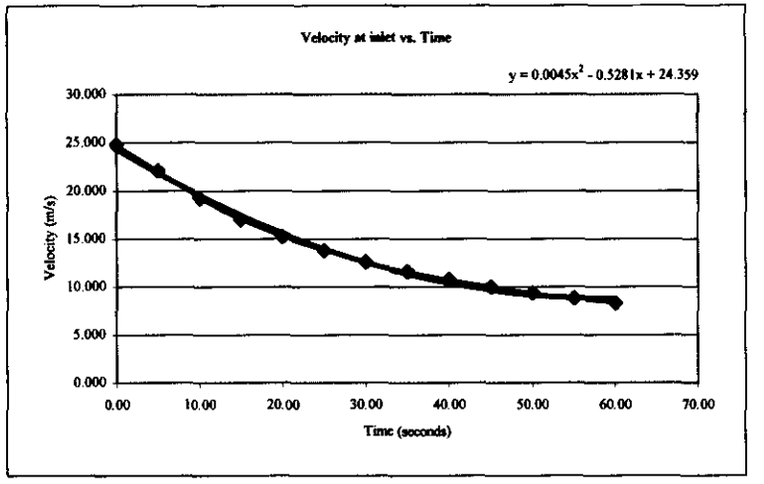

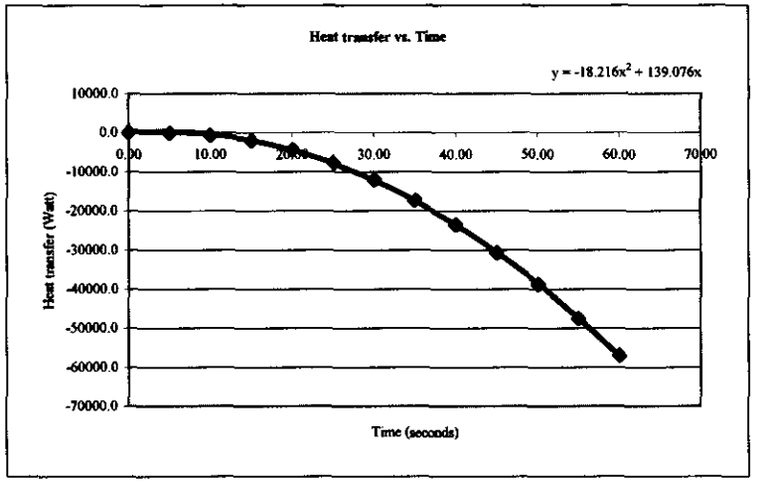

Model: No Capacitance (Reference Case)

Time seconds	Velocity m/s	Enthalpy J/kg	m.(hi+((vi)^2)/2)) J
0	24.359	631034	0.0
1	23.835	631393	5685095.3
2	23.321	631752	5688218.8
3	22.815	632112	5691346.5
4	22.319	632471	5694478.4
5	21.831	632830	5697614.2
6	21.352	633189	5700753.9
7	20.883	633548	5703897.4
8	20.422	633908	5707044.5
9	19.971	634267	5710195.1
10	19.528	634626	5713349.1
11	19.094	634985	5716506.5
12	18.670	635344	5719667.0
13	18.254	635703	5722830.7
14	17.848	636063	5725997.4
15	17.450	636422	5729166.9
16	17.061	636781	5732339.3
17	16.682	637140	5735514.3
18	16.311	637499	5738692.0
19	15.950	637859	5741872.2
20	15.597	638218	5745054.9
21	15.253	638577	5748239.9
22	14.919	638936	5751427.2
23	14.593	639295	5754616.7
24	14.277	639655	5757808.2
25	13.969	640014	5761001.8
26	13.670	640373	5764197.4
27	13.381	640732	5767394.9
28	13.100	641091	5770594.1
29	12.829	641451	5773795.2
30	12.566	641810	5776997.9
31	12.312	642169	5780202.2
32	12.068	642528	5783408.1
33	11.832	642887	5786615.4
34	11.606	643246	5789824.2
35	11.388	643606	5793034.4
36	11.179	643965	5796246.0
37	10.980	644324	5799458.8
38	10.789	644683	5802672.8
39	10.608	645042	5805888.0
40	10.435	645402	5809104.4
41	10.271	645761	5812321.9
42	10.117	646120	5815540.4
43	9.971	646479	5818759.9
44	9.835	646838	5821980.5
45	9.707	647198	5825202.0
46	9.588	647557	5828424.4
47	9.479	647916	5831647.7
48	9.378	648275	5834871.9
49	9.287	648634	5838096.9
50	9.204	648994	5841322.7
51	9.130	649353	5844549.3
52	9.066	649712	5847776.8
53	9.010	650071	5851005.0
54	8.964	650430	5854233.9
55	8.926	650789	5857463.6
56	8.897	651149	5860694.0
57	8.878	651508	5863925.1
58	8.867	651867	5867157.0
59	8.866	652226	5870389.6
60	8.873	652585	5873622.9

346731147	J	Sum[m.(hi+((vi)^2)/2))]
-1061215	J	Q
345669932	J	Sum[m.(hi+((vi)^2)/2))]+Q

Model: No Capacitance (Reference Case)

Volume m^3		Temperature K	Gauge pressure Pa	Abs Pressure Pa	Avg density kg/m^3	Enthalpy J/kg	Mass kg	Internal energy J/kg	m.u J
102.964	start	293.00	0	3019000	4.96	113456.18	510.70	-495213.17	-252906080
	end	447.85	6407123	9426123	10.11	938001.94	1040.97	5645.56	5876833

m2u2-m1u1	J	258782913

Volume m^3		Temperature K	Gauge pressure Pa	Abs Pressure Pa	Avg density kg/m^3	Enthalpy J/kg	Mass kg	Internal energy J/kg	m.u J
0.979	start	293.00	0	3019000	4.96	113456.18	4.86	-495213.17	-2404365
	end	393.31	6407210	3019011	11.45	633972.67	11.21	370303.55	4150399

m2u2-m1u1	J	6554764

Volume m^3		Temperature K	Density kg/m^3	Mass kg	Cp J/kg.K	m.Cp.T J
7.659	start	293.00	8030	61503.60	502.48	9054968500
	end	295.00				9116777158

m2u2-m1u1	J	61808659

Volume m^3		Temperature K	Density kg/m^3	Mass kg	Cp J/kg.K	m.Cp.T J
0.056	start	293.00	8030	447.34	502.48	65859664
	end	387.62				87127391

m2u2-m1u1	J	21267726

345669932	J	Sum[m.(hi+((vi)^2)/2))]+Q
348414062	J	Sum(m2u2-m1u1)
2744130	J	Difference
0.79	**%**	**Deviance**

1055.56	kg	Initial mass + mass in
1052.17	kg	End: Density.Volume
3.38	kg	Difference

Model: Capacitance

Time step	Time seconds	Temperature K	Gauge Pressure Pa	Abs Pressure Pa	Density kg/m^3	Heat transfer Watt	Velcoity m/s	Enthalpy J/kg
0	0.00	392.75	0	3019000	3.872	0.0	24.777	631066.22
500	5.00	392.75	317262	3336262	4.092	-22.6	23.446	632130.95
1000	10.00	392.75	634760	3653760	4.481	-103.1	21.413	633196.48
1500	15.00	392.75	958356	3977356	4.877	-253.5	19.673	634282.47
2000	20.00	392.75	1288240	4307240	5.281	-481.8	18.168	635389.56
2500	25.00	392.75	1624154	4643154	5.692	-794.5	16.855	636516.89
3000	30.00	392.75	1965912	4984912	6.111	-1194.7	15.700	637663.83
3500	35.00	392.75	2313320	5332320	6.537	-1684.5	14.678	638829.73
4000	40.00	392.75	2666206	5685206	6.969	-2264.8	13.767	640014.02
4500	45.00	392.75	3024391	6043391	7.408	-2936.1	12.951	641216.09
5000	50.00	392.75	3387722	6406722	7.853	-3698.2	12.217	642435.43
5500	55.00	392.75	3756025	6775025	8.305	-4550.7	11.553	643671.45
6000	60.00	392.75	4129164	7148164	8.762	-5492.8	10.950	644923.71

Model: Capacitance

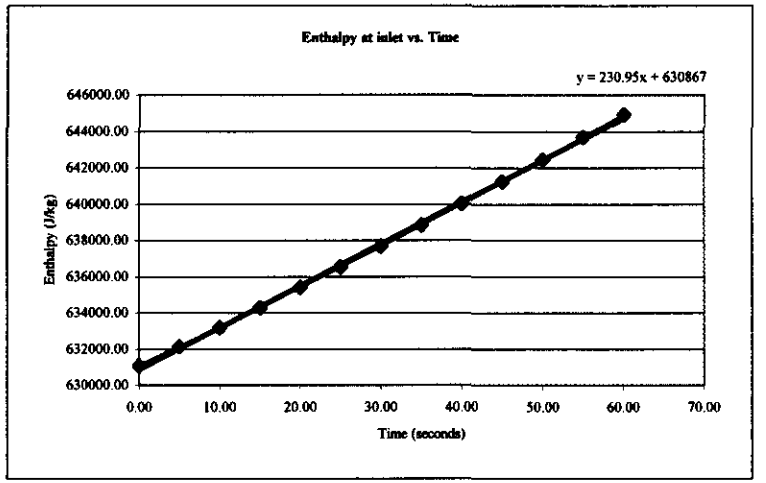

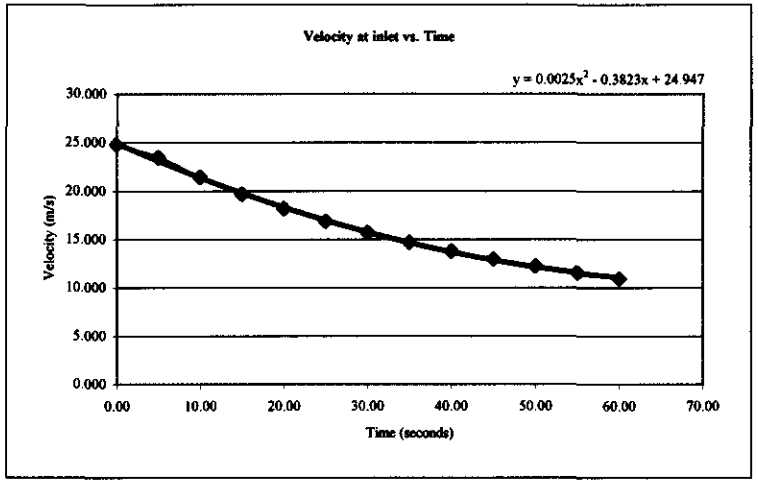

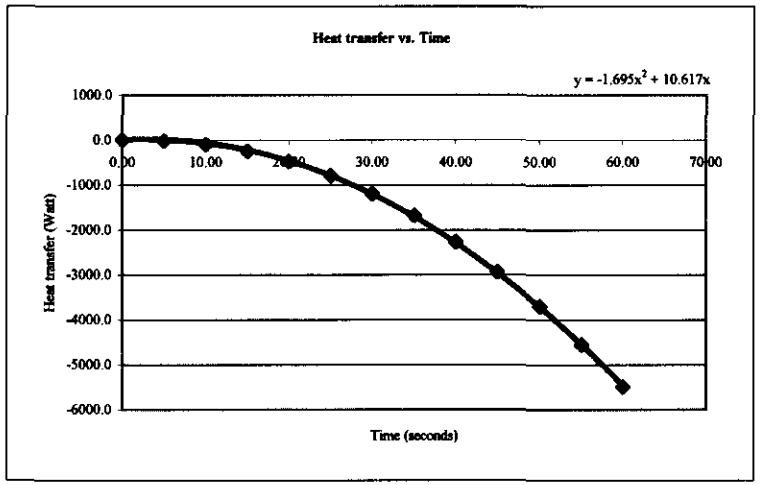

Model: Capacitance

Time seconds	Velocity m/s	Enthalpy J/kg	m.(hi+((vi)^2)/2)) J
0	24.347	630867	0.0
1	23.967	631097	5682461.1
2	23.592	631328	5684454.0
3	23.223	631558	5686449.3
4	22.858	631788	5688446.8
5	22.498	632019	5690446.5
6	22.143	632249	5692448.3
7	21.793	632479	5694452.3
8	21.449	632710	5696458.4
9	21.109	632940	5698466.5
10	20.774	633171	5700476.5
11	20.444	633401	5702488.5
12	20.119	633631	5704502.4
13	19.800	633862	5706518.1
14	19.485	634092	5708535.6
15	19.175	634322	5710554.8
16	18.870	634553	5712575.8
17	18.570	634783	5714598.4
18	18.276	635013	5716622.7
19	17.986	635244	5718648.6
20	17.701	635474	5720676.0
21	17.421	635704	5722704.9
22	17.146	635935	5724735.3
23	16.877	636165	5726767.1
24	16.612	636395	5728800.4
25	16.352	636626	5730835.0
26	16.097	636856	5732870.9
27	15.847	637086	5734908.2
28	15.603	637317	5736946.7
29	15.363	637547	5738986.4
30	15.128	637778	5741027.4
31	14.898	638008	5743069.5
32	14.673	638238	5745112.7
33	14.454	638469	5747157.0
34	14.239	638699	5749202.4
35	14.029	638929	5751248.9
36	13.824	639160	5753296.4
37	13.624	639390	5755344.9
38	13.430	639620	5757394.3
39	13.240	639851	5759444.7
40	13.055	640081	5761495.9
41	12.875	640311	5763548.1
42	12.700	640542	5765601.2
43	12.531	640772	5767655.0
44	12.366	641002	5769709.7
45	12.206	641233	5771765.2
46	12.051	641463	5773821.4
47	11.901	641693	5775878.4
48	11.757	641924	5777936.2
49	11.617	642154	5779994.6
50	11.482	642385	5782053.8
51	11.352	642615	5784113.6
52	11.227	642845	5786174.0
53	11.108	643076	5788235.2
54	10.993	643306	5790296.9
55	10.883	643536	5792359.2
56	10.778	643767	5794422.2
57	10.678	643997	5796485.7
58	10.584	644227	5798549.8
59	10.494	644458	5800614.4
60	10.409	644688	5802679.6

344533523	J	Sum[m.(hi+((vi)^2)/2))]
-98609	J	Q
344434914	J	Sum[m.(hi+((vi)^2)/2))]+Q

Model: Capacitance

Volume m^3		Temperature K	Gauge pressure Pa	Abs Pressure Pa	Avg density kg/m^3	Enthalpy J/kg	Mass kg	Internal energy J/kg	m.u J
100.390	start	293.00	0	3019000	4.96	113456.18	497.93	-495213.17	-246583428
	end	334.45	4129072	7148072	10.35	342827.40	1039.46	-347528.77	-361240547

m2u2-m1u1	J	-114657119

Volume m^3		Temperature K	Gauge pressure Pa	Abs Pressure Pa	Avg density kg/m^3	Enthalpy J/kg	Mass kg	Internal energy J/kg	m.u J
0.979	start	293.00	0	3019000	4.96	113456.18	4.86	-495213.17	-2404365
	end	392.67	4129190	7148190	8.76	644510.20	8.58	-171153.55	-1468241

m2u2-m1u1	J	936124

Volume m^3		Temperature K	Density kg/m^3	Mass kg	Cp J/kg.K	m.Cp.T J
2.574	start	293.00	8030	20670.02	502.48	3043178035
	end	334.45				3473689057

m2u2-m1u1	J	430511022.4

Volume m^3		Temperature K	Density kg/m^3	Mass kg	Cp J/kg.K	m.Cp.T J
7.659	start	293.00	8030	61503.60	502.48	9054968500
	end	293.20				9061038110

m2u2-m1u1	J	6069610.284

Volume m^3		Temperature K	Density kg/m^3	Mass kg	Cp J/kg.K	m.Cp.T J
0.056	start	293.00	8030	447.34	502.48	65859664
	end	385.76				86709980

m2u2-m1u1	J	20850316

344434914	J	Sum[m.(hi+((vi)^2)/2))]+Q
343709953	J	Sum(m2u2-m1u1)
724961	J	Difference
0.21	**%**	**Deviance**

1042.79	kg	Initial mass + mass in
1048.03	kg	End: Density.Volume
5.24	kg	Difference

Model: Concept1 - No Pipes

Time step	Time seconds	Temperature K	Gauge Pressure Pa	Abs Pressure Pa	Density kg/m^3	Heat transfer Watt	Velcoity m/s	Enthalpy J/kg
0	0.00	392.75	0	3019000	3.872	0.0	24.777	631066.22
500	5.00	392.75	314462	3333462	4.089	-18.2	23.465	632121.56
1000	10.00	392.75	633463	3652463	4.479	-105.9	21.420	633192.13
1500	15.00	392.75	958530	3977530	4.877	-296.1	19.672	634283.05
2000	20.00	392.75	1289492	4308492	5.282	-611.4	18.162	635393.76
2500	25.00	392.75	1626228	4645228	5.695	-1067.6	16.847	636523.85
3000	30.00	392.75	1968608	4987608	6.114	-1676.3	15.691	637672.88
3500	35.00	392.75	2316392	5335392	6.540	-2446.3	14.669	638840.04
4000	40.00	392.75	2669420	5688420	6.973	-3384.9	13.759	640024.80
4500	45.00	392.75	3027579	6046579	7.412	-4498.7	12.944	641226.79
5000	50.00	392.75	3390606	6409606	7.857	-5793.4	12.211	642445.11
5500	55.00	392.75	3757574	6776574	8.306	-7271.1	11.550	643676.65
6000	60.00	392.75	4129895	7148895	8.763	-8942.0	10.949	644926.16

Model: Concept1 - No Pipes

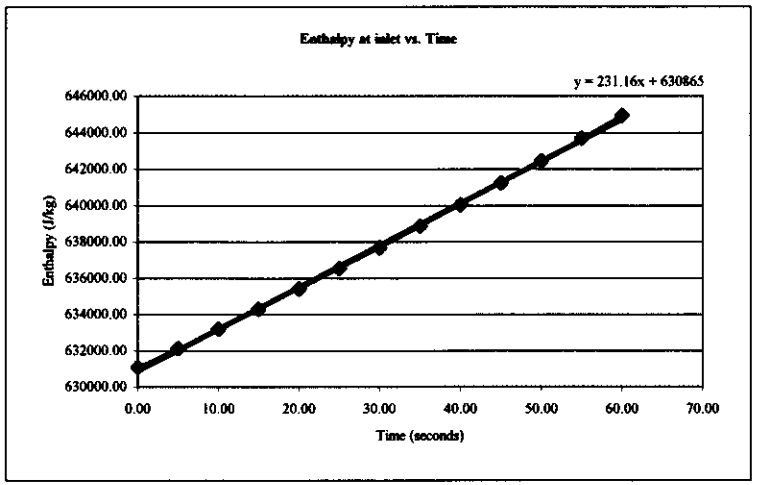

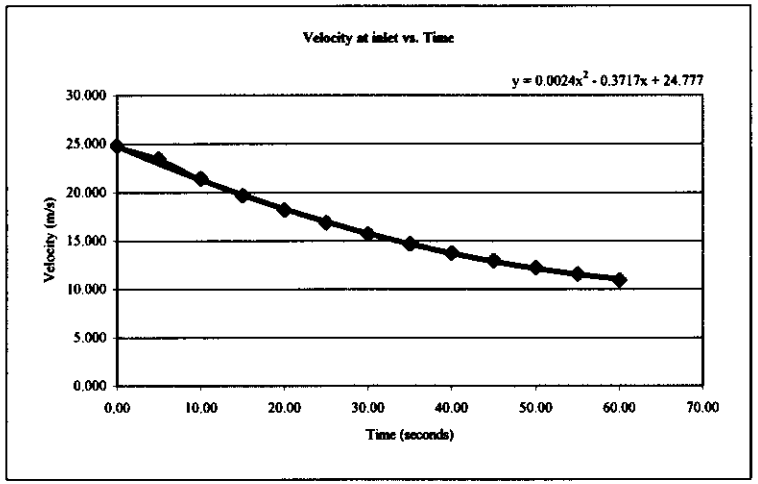

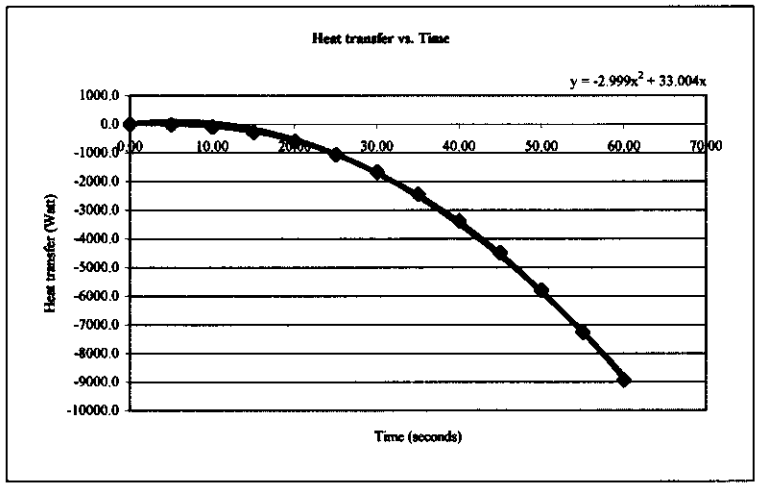

Model: Concept1 - No Pipes

Time seconds	Velocity m/s	Enthalpy J/kg	m.(hi+((vi)^2)/2)) J
0	24.777	630865	0.0
1	24.408	631096	5682546.3
2	24.043	631327	5684547.2
3	23.684	631558	5686550.4
4	23.329	631790	5688555.8
5	22.979	632021	5690563.3
6	22.633	632252	5692572.8
7	22.293	632483	5694584.4
8	21.957	632714	5696598.0
9	21.626	632945	5698613.6
10	21.300	633177	5700631.0
11	20.979	633408	5702650.3
12	20.662	633639	5704671.4
13	20.351	633870	5706694.4
14	20.044	634101	5708719.0
15	19.742	634332	5710745.4
16	19.444	634564	5712773.4
17	19.152	634795	5714803.0
18	18.864	635026	5716834.2
19	18.581	635257	5718867.0
20	18.303	635488	5720901.3
21	18.030	635719	5722937.1
22	17.761	635951	5724974.3
23	17.498	636182	5727012.9
24	17.239	636413	5729052.8
25	16.985	636644	5731094.1
26	16.735	636875	5733136.7
27	16.491	637106	5735180.6
28	16.251	637337	5737225.7
29	16.016	637569	5739272.1
30	15.786	637800	5741319.6
31	15.561	638031	5743368.2
32	15.340	638262	5745418.0
33	15.125	638493	5747468.9
34	14.914	638724	5749520.8
35	14.708	638956	5751573.8
36	14.506	639187	5753627.8
37	14.310	639418	5755682.7
38	14.118	639649	5757738.7
39	13.931	639880	5759795.5
40	13.749	640111	5761853.3
41	13.572	640343	5763911.9
42	13.399	640574	5765971.4
43	13.232	640805	5768031.7
44	13.069	641036	5770092.9
45	12.911	641267	5772154.9
46	12.757	641498	5774217.6
47	12.609	641730	5776281.1
48	12.465	641961	5778345.3
49	12.326	642192	5780410.3
50	12.192	642423	5782475.9
51	12.063	642654	5784542.2
52	11.938	642885	5786609.2
53	11.819	643116	5788676.9
54	11.704	643348	5790745.1
55	11.594	643579	5792814.0
56	11.488	643810	5794883.5
57	11.388	644041	5796953.6
58	11.292	644272	5799024.3
59	11.201	644503	5801095.6
60	11.115	644315	5799394.5

344547308	J	Sum[m.(hi+((vi)^2)/2))]
-156521	J	Q
344390787	J	Sum[m.(hi+((vi)^2)/2))]+Q

Model: Capacitance

FLUID - Internal energy deviation

Helium in Tank									
Volume m^3		Temperature K	Gauge pressure Pa	Abs Pressure Pa	Avg density kg/m^3	Enthalpy J/kg	Mass kg	Internal energy J/kg	m.u J
100.390	start	293.00	0	3019000	4.96	113456.18	497.93	-495213.17	-246583428
	end	334.45	4129072	7148072	10.35	342827.40	1039.46	-347528.77	-361240547
							m2u2-m1u1	J	-114657119

Helium in Pipe									
Volume m^3		Temperature K	Gauge pressure Pa	Abs Pressure Pa	Avg density kg/m^3	Enthalpy J/kg	Mass kg	Internal energy J/kg	m.u J
0.979	start	293.00	0	3019000	4.96	113456.18	4.86	-495213.17	-2404365
	end	392.67	4129190	7148190	8.76	644510.20	8.58	-171153.55	-1468241
							m2u2-m1u1	J	936124

SOLID material - Internal energy deviation

Capacitance						
Volume m^3		Temperature K	Density kg/m^3	Mass kg	Cp J/kg.K	m.Cp.T J
2.574	start	293.00	8030	20670.02	502.48	3043178035
	end	334.45				3473689057
					m2u2-m1u1	J	430511022.4

Tank						
Volume m^3		Temperature K	Density kg/m^3	Mass kg	Cp J/kg.K	m.Cp.T J
7.659	start	293.00	8030	61503.60	502.48	9054968500
	end	293.20				9061038110
					m2u2-m1u1	J	6069610.284

Pipe						
Volume m^3		Temperature K	Density kg/m^3	Mass kg	Cp J/kg.K	m.Cp.T J
0.056	start	293.00	8030	447.34	502.48	65859664
	end	385.76				86709980
					m2u2-m1u1	J	20850316

Energy conservation		
344434914	J	Sum[m.(hi+((vi)^2)/2))]+Q
343709953	J	Sum(m2u2-m1u1)
724961	J	Difference
0.21	%	Deviance

Mass conservation		
1042.79	kg	Initial mass + mass in
1048.03	kg	End: Density.Volume
5.24	kg	Difference
0.50	%	Deviance

Model: Concept1 - No Pipes

Conditions at model inlet								
Time step	Time seconds	Temperature K	Gauge Pressure Pa	Abs Pressure Pa	Density kg/m^3	Heat transfer Watt	Velcoity m/s	Enthalpy J/kg
0	0.00	392.75	0	3019000	3.872	0.0	24.777	631066.22
500	5.00	392.75	314462	3333462	4.089	-18.2	23.465	632121.56
1000	10.00	392.75	633463	3652463	4.479	-105.9	21.420	633192.13
1500	15.00	392.75	958530	3977530	4.877	-296.1	19.672	634283.05
2000	20.00	392.75	1289492	4308492	5.282	-611.4	18.162	635393.76
2500	25.00	392.75	1626228	4645228	5.695	-1067.6	16.847	636523.85
3000	30.00	392.75	1968608	4987608	6.114	-1676.3	15.691	637672.88
3500	35.00	392.75	2316392	5335392	6.540	-2446.3	14.669	638840.04
4000	40.00	392.75	2669420	5688420	6.973	-3384.9	13.759	640024.80
4500	45.00	392.75	3027579	6046579	7.412	-4498.7	12.944	641226.79
5000	50.00	392.75	3390606	6409606	7.857	-5793.4	12.211	642445.11
5500	55.00	392.75	3757574	6776574	8.306	-7271.1	11.550	643676.65
6000	60.00	392.75	4129895	7148895	8.763	-8942.0	10.949	644926.16

Model: Concept1 - No Pipes

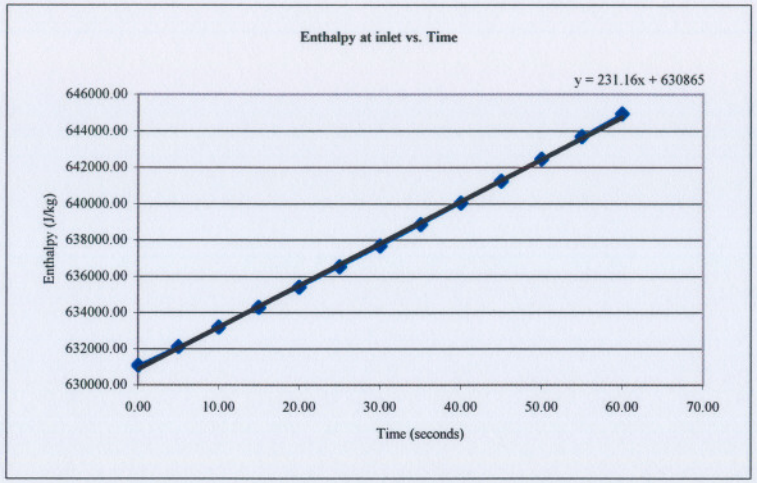

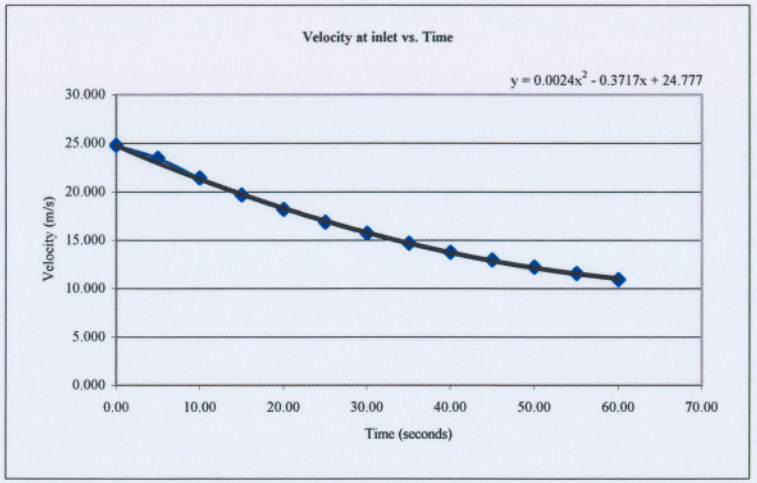

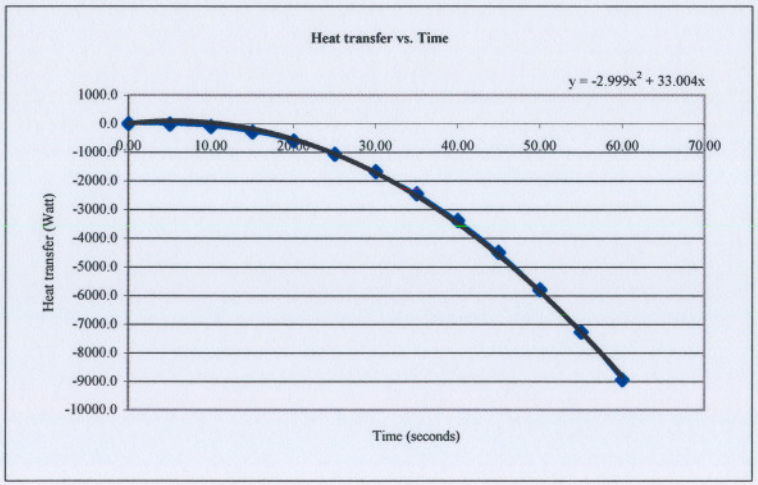

Model: Concept1 - No Pipes

Time seconds	Velocity m/s	Enthalpy J/kg	m.(hi+((vi)^2)/2)) J
0	24.777	630865	0.0
1	24.408	631096	5682546.3
2	24.043	631327	5684547.2
3	23.684	631558	5686550.4
4	23.329	631790	5688555.8
5	22.979	632021	5690563.3
6	22.633	632252	5692572.8
7	22.293	632483	5694584.4
8	21.957	632714	5696598.0
9	21.626	632945	5698613.6
10	21.300	633177	5700631.0
11	20.979	633408	5702650.3
12	20.662	633639	5704671.4
13	20.351	633870	5706694.4
14	20.044	634101	5708719.0
15	19.742	634332	5710745.4
16	19.444	634564	5712773.4
17	19.152	634795	5714803.0
18	18.864	635026	5716834.2
19	18.581	635257	5718867.0
20	18.303	635488	5720901.3
21	18.030	635719	5722937.1
22	17.761	635951	5724974.3
23	17.498	636182	5727012.9
24	17.239	636413	5729052.8
25	16.985	636644	5731094.1
26	16.735	636875	5733136.7
27	16.491	637106	5735180.6
28	16.251	637337	5737225.7
29	16.016	637569	5739272.1
30	15.786	637800	5741319.6
31	15.561	638031	5743368.2
32	15.340	638262	5745418.0
33	15.125	638493	5747468.9
34	14.914	638724	5749520.8
35	14.708	638956	5751573.8
36	14.506	639187	5753627.8
37	14.310	639418	5755682.7
38	14.118	639649	5757738.7
39	13.931	639880	5759795.5
40	13.749	640111	5761853.3
41	13.572	640343	5763911.9
42	13.399	640574	5765971.4
43	13.232	640805	5768031.7
44	13.069	641036	5770092.9
45	12.911	641267	5772154.9
46	12.757	641498	5774217.6
47	12.609	641730	5776281.1
48	12.465	641961	5778345.3
49	12.326	642192	5780410.3
50	12.192	642423	5782475.9
51	12.063	642654	5784542.2
52	11.938	642885	5786609.2
53	11.819	643116	5788676.9
54	11.704	643348	5790745.1
55	11.594	643579	5792814.0
56	11.488	643810	5794883.5
57	11.388	644041	5796953.6
58	11.292	644272	5799024.3
59	11.201	644503	5801095.6
60	11.115	644315	5799394.5

344547308	J	Sum[m.(hi+((vi)^2)/2))]
-156521	J	Q
344390787	J	Sum[m.(hi+((vi)^2)/2))]+Q

Model: Concept1 - No Pipes

FLUID - Internal energy deviation

Helium in Tank									
Volume m^3		Temperature K	Gauge pressure Pa	Abs Pressure Pa	Avg density kg/m^3	Enthalpy J/kg	Mass kg	Internal energy J/kg	m.u J
101.315	start	293.00	0	3019000	4.96	113456.18	502.52	-495213.17	-248856381
	end	335.21	4129496	7148496	10.34	346765.98	1047.60	-344577.93	-360979806
							m2u2-m1u1	J	-112123425

Helium in Pipe									
Volume m^3		Temperature K	Gauge pressure Pa	Abs Pressure Pa	Avg density kg/m^3	Enthalpy J/kg	Mass kg	Internal energy J/kg	m.u J
0.086	start	293.00	0	3019000	4.96	113456.18	0.43	-495213.17	-212299
	end	392.76	4129883	7148883	8.76	644991.95	0.76	-170868.28	-129407
							m2u2-m1u1	J	82892

SOLID material - Internal energy deviation

Capacitance						
Volume m^3		Temperature K	Density kg/m^3	Mass kg	Cp J/kg.K	m.Cp.T J
2.598	start	293.00	8030	20860.55	502.48	3071229395
	end	335.21				3513675105
				m2u2-m1u1	J	442445709.1

Tank						
Volume m^3		Temperature K	Density kg/m^3	Mass kg	Cp J/kg.K	m.Cp.T J
7.663	start	293.00	8030	61536.08	502.48	9059750620
	end	293.35				9070483177
				m2u2-m1u1	J	10732557.82

Pipe						
Volume m^3		Temperature K	Density kg/m^3	Mass kg	Cp J/kg.K	m.Cp.T J
0.0048	start	293.00	8030	38.20	502.48	5624127
	end	388.53				7457907
				m2u2-m1u1	J	1833780

Energy conservation		
344390787	J	Sum[m.(hi+((vi)^2)/2))]+Q
342971514	J	Sum(m2u2-m1u1)
1419273	J	Difference
0.41	%	Deviance

Mass conservation		
1042.95	kg	Initial mass + mass in
1048.36	kg	End: Density.Volume
5.40	kg	Difference
0.52	%	Deviance

Model: Concept2 - 3 Pipes

Conditions at model inlet								
Time step	Time seconds	Temperature K	Gauge Pressure Pa	Abs Pressure Pa	Density kg/m^3	Heat transfer Watt	Velcoity m/s	Enthalpy J/kg
0	0.00	392.75	0	3019000	3.872	0.0	14.797	631066.22
500	3.33	392.75	215801	3234801	3.967	-8.5	14.442	631790.45
1000	8.33	392.75	531114	3550114	4.354	-64.9	13.162	632848.64
1500	13.33	392.75	852792	3871792	4.747	-185.8	12.069	633928.19
2000	18.33	392.75	1180700	4199700	5.149	-379.7	11.128	635028.66
2500	23.33	392.75	1514653	4533653	5.558	-654.4	10.309	636149.40
3000	28.33	392.75	1854475	4873475	5.974	-1014.6	9.591	637289.85
3500	33.33	392.75	2199994	5218994	6.398	-1463.7	8.956	638449.41
4000	38.33	392.75	2551041	5570041	6.828	-2004.4	8.392	639627.52
4500	43.33	392.75	2907452	5926452	7.265	-2638.5	7.887	640823.64
5000	48.33	392.75	3269065	6288065	7.708	-3367.3	7.434	642037.21
5500	53.33	392.75	3635719	6654719	8.157	-4191.5	7.025	643267.71
6146	60.00	392.75	4116267	7135267	8.746	-5398.6	6.552	644880.43

Model: Concept2 - 3 Pipes

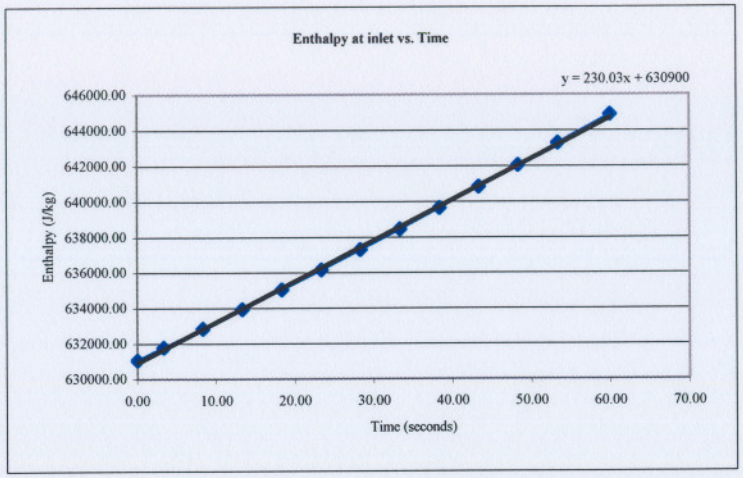

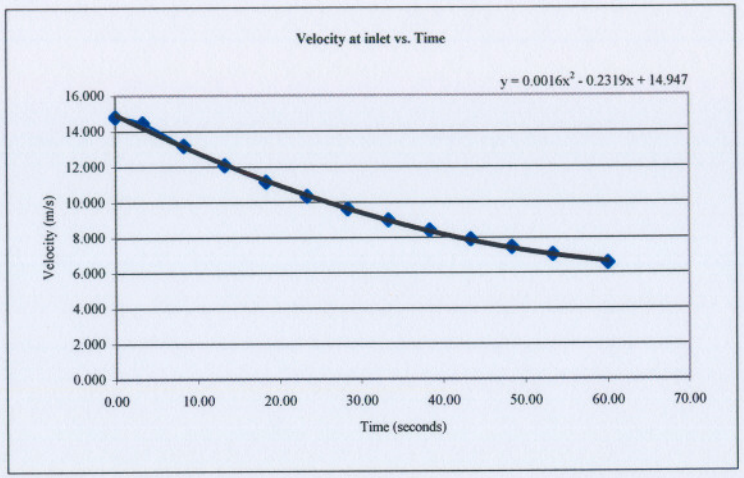

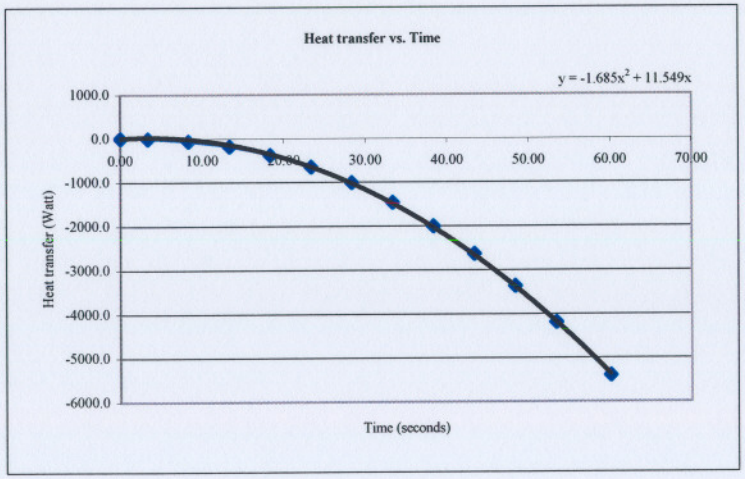

Model: Concept2 - 3 Pipes

Time seconds	Velocity m/s	Enthalpy J/kg	m.(hi+((vi)^2)/2)) J
0	14.947	630900	0.0
1	14.717	631130	5681144.9
2	14.490	631360	5683185.3
3	14.266	631590	5685226.6
4	14.045	631820	5687268.8
5	13.828	632050	5689311.7
6	13.613	632280	5691355.6
7	13.402	632510	5693400.2
8	13.194	632740	5695445.6
9	12.990	632970	5697491.7
10	12.788	633200	5699538.6
11	12.590	633430	5701586.2
12	12.395	633660	5703634.6
13	12.203	633890	5705683.6
14	12.014	634120	5707733.3
15	11.829	634350	5709783.7
16	11.646	634580	5711834.7
17	11.467	634811	5713886.3
18	11.291	635041	5715938.6
19	11.119	635271	5717991.4
20	10.949	635501	5720044.9
21	10.783	635731	5722098.9
22	10.620	635961	5724153.4
23	10.460	636191	5726208.5
24	10.303	636421	5728264.2
25	10.150	636651	5730320.3
26	9.999	636881	5732376.9
27	9.852	637111	5734434.1
28	9.708	637341	5736491.7
29	9.568	637571	5738549.7
30	9.430	637801	5740608.3
31	9.296	638031	5742667.2
32	9.165	638261	5744726.6
33	9.037	638491	5746786.4
34	8.912	638721	5748846.6
35	8.791	638951	5750907.2
36	8.672	639181	5752968.2
37	8.557	639411	5755029.5
38	8.445	639641	5757091.2
39	8.337	639871	5759153.3
40	8.231	640101	5761215.7
41	8.129	640331	5763278.4
42	8.030	640561	5765341.5
43	7.934	640791	5767404.9
44	7.841	641021	5769468.5
45	7.752	641251	5771532.5
46	7.665	641481	5773596.8
47	7.582	641711	5775661.4
48	7.502	641941	5777726.2
49	7.426	642171	5779791.4
50	7.352	642402	5781856.7
51	7.282	642632	5783922.4
52	7.215	642862	5785988.3
53	7.151	643092	5788054.4
54	7.090	643322	5790120.8
55	7.033	643552	5792187.4
56	6.978	643782	5794254.2
57	6.927	644012	5796321.3
58	6.879	644242	5798388.6
59	6.835	644472	5800456.1
60	6.793	644702	5802523.9

344502260	J	Sum[m.(hi+((vi)^2)/2))]
-100532	J	Q
344401728	J	Sum[m.(hi+((vi)^2)/2))]+Q

Model: Concept2 - 3 Pipes

FLUID - Internal energy deviation

Helium in Tank									
Volume m^3		Temperature K	Gauge pressure Pa	Abs Pressure Pa	Avg density kg/m^3	Enthalpy J/kg	Mass kg	Internal energy J/kg	m.u J
100.131	start	293.00	0	3019000	4.96	113456.18	496.65	-495213.17	-245946398
	end	334.45	4116198	7135198	10.29	342782.78	1029.87	-350949.01	-361430714
							m2u2-m1u1	J	-115484316

Helium in Pipe									
Volume m^3		Temperature K	Gauge pressure Pa	Abs Pressure Pa	Avg density kg/m^3	Enthalpy J/kg	Mass kg	Internal energy J/kg	m.u J
1.289	start	293.00	0	3019000	4.96	113456.18	6.39	-495213.17	-3166062
	end	392.98	4116278	7135278	8.74	646048.19	11.27	-170243.09	-1918142
							m2u2-m1u1	J	1247920

SOLID material - Internal energy deviation

Capacitance						
Volume m^3		Temperature K	Density kg/m^3	Mass kg	Cp J/kg.K	m.Cp.T J
2.567	start	293.00	8030	20616.62	502.48	3035316206
	end	334.45				3464715035
				m2u2-m1u1	J	429398828

Tank						
Volume m^3		Temperature K	Density kg/m^3	Mass kg	Cp J/kg.K	m.Cp.T J
7.651	start	293.00	8030	61434.92	502.48	9044856887
	end	293.19				9050870328
				m2u2-m1u1	J	6013441

Pipe						
Volume m^3		Temperature K	Density kg/m^3	Mass kg	Cp J/kg.K	m.Cp.T J
0.063	start	293.00	8030	506.96	502.48	74638715
	end	379.33				96629139
				m2u2-m1u1	J	21990425

Energy conservation		
344401728	J	Sum[m.(hi+((vi)^2)/2))]+Q
343166298	J	Sum(m2u2-m1u1)
1235430	J	Difference
0.36	%	Deviance

Mass conservation		
1043.04	kg	Initial mass + mass in
1041.13	kg	End: Density.Volume
1.91	kg	Difference
0.18	%	Deviance

Model: Concept3 - 3 Holes

Conditions at model inlet								
Time step	Time seconds	Temperature K	Gauge Pressure Pa	Abs Pressure Pa	Density kg/m^3	Heat transfer Watt	Velcoity m/s	Enthalpy J/kg
0	0.00	392.75	0	3019000	3.872	0.00	24.777	631066.22
500	5.00	392.75	317166	3336166	4.099	-20.28	23.407	632130.63
1000	10.00	392.75	633483	3652483	4.488	-84.29	21.377	633192.19
1500	15.00	392.75	955793	3974793	4.884	-206.49	19.643	634273.87
2000	20.00	392.75	1283822	4302822	5.287	-396.27	18.146	635374.73
2500	25.00	392.75	1617539	4636539	5.697	-659.75	16.840	636494.69
3000	30.00	392.75	1956814	4975814	6.114	-1001.12	15.692	637633.30
3500	35.00	392.75	2301966	5320966	6.538	-1423.22	14.674	638791.63
4000	40.00	392.75	2652777	5671777	6.969	-1927.98	13.767	639968.95
4500	45.00	392.75	3008707	6027707	7.406	-2516.60	12.954	641163.45
5000	50.00	392.75	3369593	6388593	7.850	-3189.69	12.222	642374.59
5500	55.00	392.75	3735275	6754275	8.299	-3947.34	11.561	643601.82
6000	60.00	392.75	4104525	7123525	8.753	-4789.23	10.961	644841.02

Model: Concept3 - 3 Holes

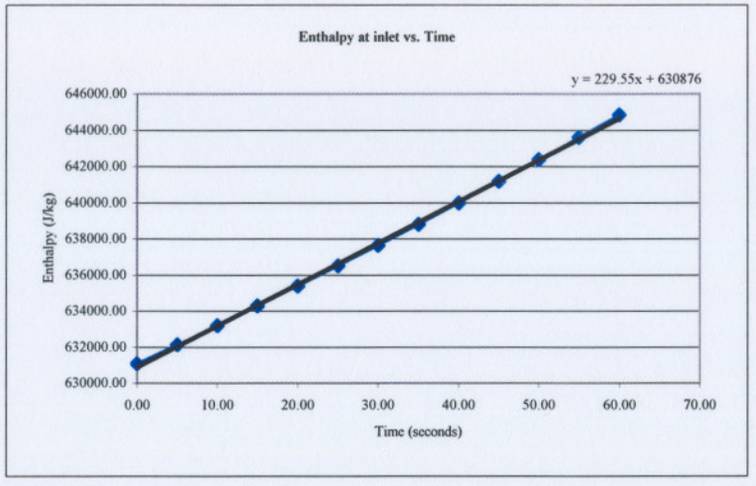

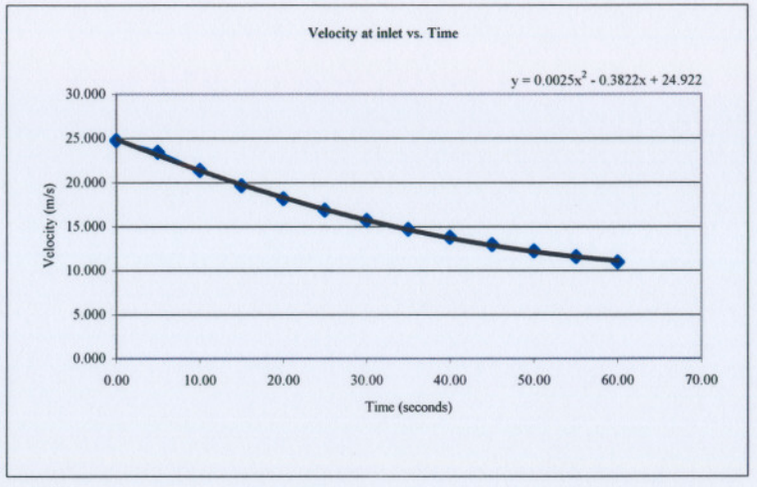

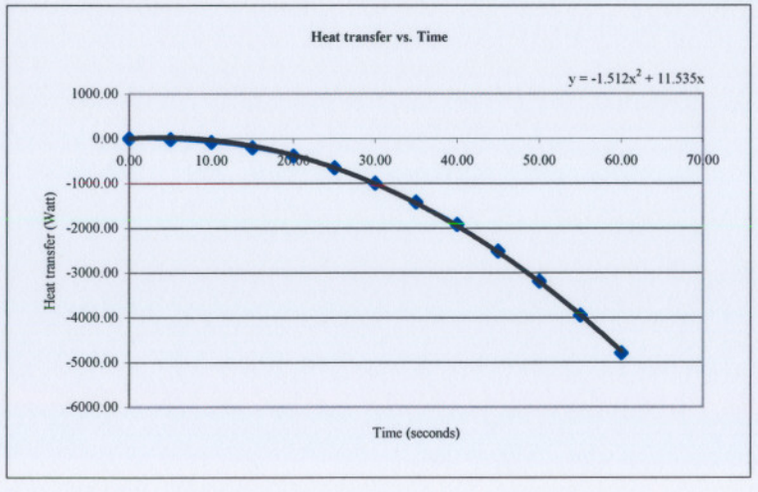

Model: Concept3 - 3 Holes

Time seconds	Velocity m/s	Enthalpy J/kg	m.(hi+((vi)^2)/2)) J
0	24.922	630876	0.0
1	24.542	631106	5682660.4
2	24.168	631335	5684644.2
3	23.798	631565	5686630.4
4	23.433	631794	5688618.8
5	23.074	632024	5690609.5
6	22.719	632253	5692602.3
7	22.369	632483	5694597.3
8	22.024	632712	5696594.4
9	21.685	632942	5698593.6
10	21.350	633172	5700594.7
11	21.020	633401	5702597.8
12	20.696	633631	5704602.8
13	20.376	633860	5706609.6
14	20.061	634090	5708618.3
15	19.752	634319	5710628.8
16	19.447	634549	5712641.0
17	19.147	634778	5714654.9
18	18.852	635008	5716670.5
19	18.563	635237	5718687.6
20	18.278	635467	5720706.4
21	17.998	635697	5722726.7
22	17.724	635926	5724748.5
23	17.454	636156	5726771.7
24	17.189	636385	5728796.4
25	16.930	636615	5730822.5
26	16.675	636844	5732849.9
27	16.425	637074	5734878.7
28	16.180	637303	5736908.7
29	15.941	637533	5738940.0
30	15.706	637763	5740972.6
31	15.476	637992	5743006.3
32	15.252	638222	5745041.2
33	15.032	638451	5747077.2
34	14.817	638681	5749114.3
35	14.608	638910	5751152.5
36	14.403	639140	5753191.7
37	14.203	639369	5755231.9
38	14.008	639599	5757273.2
39	13.819	639828	5759315.4
40	13.634	640058	5761358.5
41	13.454	640288	5763402.5
42	13.280	640517	5765447.5
43	13.110	640747	5767493.3
44	12.945	640976	5769539.9
45	12.786	641206	5771587.4
46	12.631	641435	5773635.6
47	12.481	641665	5775684.7
48	12.336	641894	5777734.4
49	12.197	642124	5779785.0
50	12.062	642354	5781836.2
51	11.932	642583	5783888.2
52	11.808	642813	5785940.8
53	11.688	643042	5787994.1
54	11.573	643272	5790048.0
55	11.464	643501	5792102.6
56	11.359	643731	5794157.8
57	11.259	643960	5796213.6
58	11.164	644190	5798270.0
59	11.075	644419	5800327.0
60	10.990	644649	5802384.5

344530214	J	Sum[m.(hi+((vi)^2)/2))]
-88101	J	Q
344442113	J	Sum[m.(hi+((vi)^2)/2))]+Q

Model: Concept3 - 3 Holes

FLUID - Internal energy deviation

Helium in Tank

Volume m^3		Temperature K	Gauge pressure Pa	Abs Pressure Pa	Avg density kg/m^3	Enthalpy J/kg	Mass kg	Internal energy J/kg	m.u J
100.395	start	293.00	0	3019000	4.96	113456.18	497.96	-495213.17	-246595402
	end	334.88	4104490	7123490	10.34	344969.80	1037.89	-344083.68	-357120737

m2u2-m1u1	J	-110525335

Helium in Pipe

Volume m^3		Temperature K	Gauge pressure Pa	Abs Pressure Pa	Avg density kg/m^3	Enthalpy J/kg	Mass kg	Internal energy J/kg	m.u J
0.979	start	293.00	0	3019000	4.96	113456.18	4.86	-495213.17	-2405834
	end	385.91	4104624	7123624	8.89	609370.31	8.71	-192084.26	-1672267

m2u2-m1u1	J	733567

SOLID material - Internal energy deviation

Capacitance

Volume m^3		Temperature K	Density kg/m^3	Mass kg	Cp J/kg.K	m.Cp.T J
2.574	start	293.00	8030	20671.03	502.48	3043325814
	end	334.88				3478324056

m2u2-m1u1	J	434998243

Tank

Volume m^3		Temperature K	Density kg/m^3	Mass kg	Cp J/kg.K	m.Cp.T J
7.663	start	293.00	8030	61530.13	502.48	9058874587
	end	293.18				9064399573

m2u2-m1u1	J	5524985.97

Pipe

Volume m^3		Temperature K	Density kg/m^3	Mass kg	Cp J/kg.K	m.Cp.T J
0.055	start	293.00	8030	442.53	502.48	65151982
	end	347.17				77197382

m2u2-m1u1	J	12045401

Energy conservation

344442113	J	Sum[m.(hi+((vi)^2)/2))]+Q
342776861	J	Sum(m2u2-m1u1)
1665252	J	Difference
0.48	%	Deviance

Mass conservation

1042.82	kg	Initial mass + mass in
1046.60	kg	End: Density.Volume
3.78	kg	Difference
0.36	%	Deviance

Model: Sensitivity (+10%)

Conditions at model inlet								
Time step	Time seconds	Temperature K	Gauge Pressure Pa	Abs Pressure Pa	Density kg/m^3	Heat transfer Watt	Velcoity m/s	Enthalpy J/kg
0	0.00	392.75	0	3019000	3.872235	0.0	24.777	631066.22
500	5.00	392.75	317341	3336341	4.092093	-22.5	23.446	632131.22
1000	10.00	392.75	634661	3653661	4.480477	-102.8	21.413	633196.15
1500	15.00	392.75	958435	3977435	4.876892	-252.2	19.673	634282.73
2000	20.00	392.75	1288346	4307346	5.280925	-478.0	18.167	635389.92
2500	25.00	392.75	1624282	4643282	5.692418	-786.6	16.854	636517.32
3000	30.00	392.75	1966052	4985052	6.11112	-1181.3	15.699	637664.30
3500	35.00	392.75	2313478	5332478	6.5368	-1664.5	14.677	638830.26
4000	40.00	392.75	2666381	5685381	6.969229	-2237.3	13.766	640014.61
4500	45.00	392.75	3024595	6043595	7.408194	-2900.3	12.951	641216.77
5000	50.00	392.75	3387962	6406962	7.853497	-3653.5	12.216	642436.23
5500	55.00	392.75	3756319	6775319	8.304931	-4496.5	11.552	643672.44
6000	60.00	392.75	4129508	7148508	8.7623	-5428.9	10.949	644924.86

Model: Sensitivity (+10%)

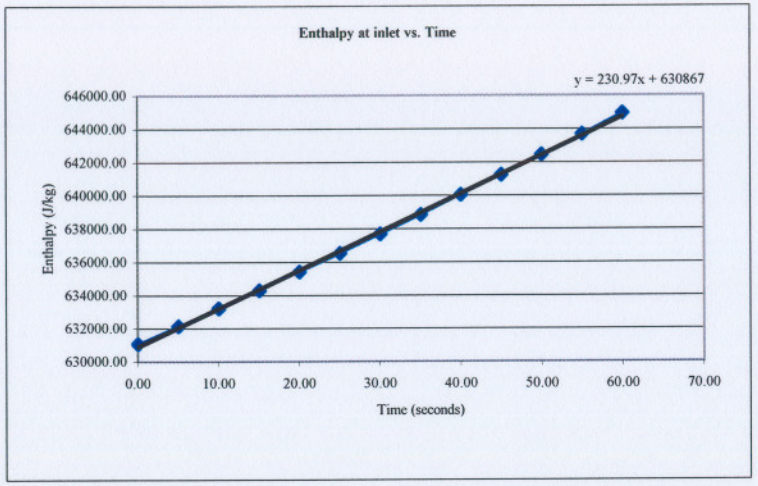

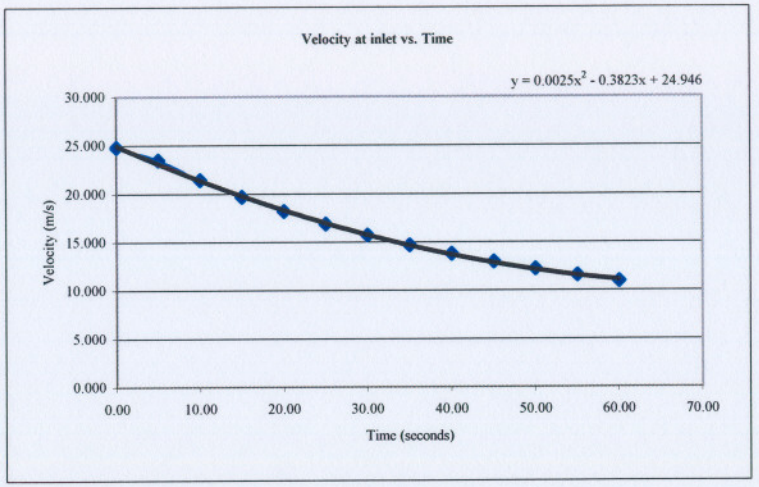

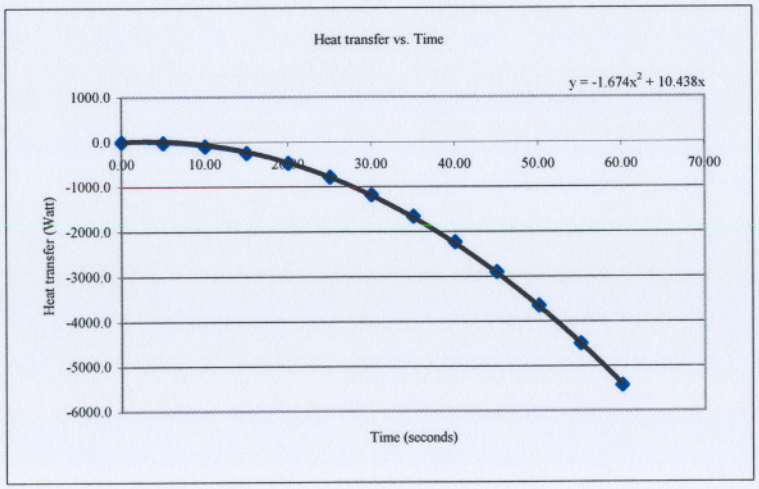

Model: Sensitivity (+10%)

Time seconds	Velocity m/s	Enthalpy J/kg	m.(hi+((vi)^2)/2)) J
0	24.346	630867	0.0
1	23.966	631098	5682466.4
2	23.591	631329	5684465.0
3	23.222	631560	5686465.8
4	22.857	631791	5688468.9
5	22.497	632022	5690474.2
6	22.142	632253	5692481.6
7	21.792	632484	5694491.2
8	21.448	632715	5696502.8
9	21.108	632946	5698516.5
10	20.773	633177	5700532.1
11	20.443	633408	5702549.7
12	20.118	633639	5704569.1
13	19.799	633870	5706590.4
14	19.484	634101	5708613.5
15	19.174	634332	5710638.3
16	18.869	634563	5712664.9
17	18.569	634793	5714693.1
18	18.275	635024	5716723.0
19	17.985	635255	5718754.4
20	17.700	635486	5720787.4
21	17.420	635717	5722821.9
22	17.145	635948	5724857.9
23	16.876	636179	5726895.3
24	16.611	636410	5728934.2
25	16.351	636641	5730974.3
26	16.096	636872	5733015.9
27	15.846	637103	5735058.7
28	15.602	637334	5737102.8
29	15.362	637565	5739148.1
30	15.127	637796	5741194.6
31	14.897	638027	5743242.3
32	14.672	638258	5745291.1
33	14.453	638489	5747341.0
34	14.238	638720	5749392.0
35	14.028	638951	5751444.1
36	13.823	639182	5753497.1
37	13.623	639413	5755551.2
38	13.429	639644	5757606.2
39	13.239	639875	5759662.2
40	13.054	640106	5761719.0
41	12.874	640337	5763776.8
42	12.699	640568	5765835.4
43	12.530	640799	5767894.8
44	12.365	641030	5769955.1
45	12.205	641261	5772016.2
46	12.050	641492	5774078.0
47	11.900	641723	5776140.6
48	11.756	641954	5778203.9
49	11.616	642185	5780267.9
50	11.481	642416	5782332.7
51	11.351	642646	5784398.1
52	11.226	642877	5786464.1
53	11.107	643108	5788530.8
54	10.992	643339	5790598.1
55	10.882	643570	5792666.0
56	10.777	643801	5794734.5
57	10.677	644032	5796803.6
58	10.583	644263	5798873.3
59	10.493	644494	5800943.5
60	10.408	644725	5803014.3

344543726	J	Sum[m.(hi+((vi)^2)/2))]
-101740	J	Q
344441987	J	Sum[m.(hi+((vi)^2)/2))]+Q

Model: Sensitivity (+10%)

FLUID - Internal energy deviation

Helium in Tank

Volume m^3		Temperature K	Gauge pressure Pa	Abs Pressure Pa	Avg density kg/m^3	Enthalpy J/kg	Mass kg	Internal energy J/kg	m.u J
100.390	start	293.00	0	3019000	4.96	113456.18	497.93	-495213.17	-246583428
	end	334.18	4129416	7148416	10.35	341429.89	1039.47	-348948.17	-362721905

m2u2-m1u1	J	-116138477

Helium in Pipe

Volume m^3		Temperature K	Gauge pressure Pa	Abs Pressure Pa	Avg density kg/m^3	Enthalpy J/kg	Mass kg	Internal energy J/kg	m.u J
0.979	start	293.00	0	3019000	4.96	113456.18	4.86	-495213.17	-2404365
	end	392.67	4129534	3019009	8.76	630673.37	8.58	286194.14	2455209

m2u2-m1u1	J	4859574

SOLID material - Internal energy deviation

Capacitance

Volume m^3		Temperature K	Density kg/m^3	Mass kg	Cp J/kg.K	m.Cp.T J
2.574	start	293.00	8030	20670.02	502.48	3043178035
	end	334.18				3470884764

m2u2-m1u1	J	427706729

Tank

Volume m^3		Temperature K	Density kg/m^3	Mass kg	Cp J/kg.K	m.Cp.T J
7.659	start	293.00	8030	61503.60	502.48	9054968500
	end	293.19				9060970120

m2u2-m1u1	J	6001621

Pipe

Volume m^3		Temperature K	Density kg/m^3	Mass kg	Cp J/kg.K	m.Cp.T J
0.056	start	293.00	8030	447.34	502.48	65859664
	end	383.91				86293333

m2u2-m1u1	J	20433669

Energy conservation

344441987	J	Sum[m.(hi+((vi)^2)/2))]+Q
342863116	J	Sum(m2u2-m1u1)
1578871	J	Difference
0.46	%	Deviance

Mass conservation

1042.79	kg	Initial mass + mass in
1048.05	kg	End: Density.Volume
5.26	kg	Difference
0.50	%	Deviance

Model: Sensitivity (-10%)

Conditions at model inlet								
Time step	Time seconds	Temperature K	Gauge Pressure Pa	Abs Pressure Pa	Density kg/m^3	Heat transfer Watt	Velcoity m/s	Enthalpy J/kg
0	0.00	392.75	0	3019000	3.872	0.0	24.777	631066.22
500	5.00	392.75	316396	3335396	4.091	-22.7	23.452	632128.05
1000	10.00	392.75	633029	3652029	4.478	-105.3	21.423	633190.67
1500	15.00	392.75	956489	3975489	4.875	-261.9	19.682	634276.20
2000	20.00	392.75	1286283	4305283	5.278	-500.6	18.176	635382.99
2500	25.00	392.75	1622099	4641099	5.690	-827.3	16.862	636509.99
3000	30.00	392.75	1963746	4982746	6.108	-1244.4	15.707	637656.56
3500	35.00	392.75	2311040	5330040	6.534	-1753.6	14.684	638822.08
4000	40.00	392.75	2663806	5682806	6.966	-2355.3	13.773	640005.96
4500	45.00	392.75	3021875	6040875	7.405	-3049.7	12.957	641207.64
5000	50.00	392.75	3385089	6404089	7.850	-3836.4	12.222	642426.59
5500	55.00	392.75	3753286	6772286	8.301	-4714.6	11.557	643662.26
6000	60.00	392.75	4126307	7145307	8.758	-5683.4	10.954	644914.12

Model: Sensitivity (-10%)

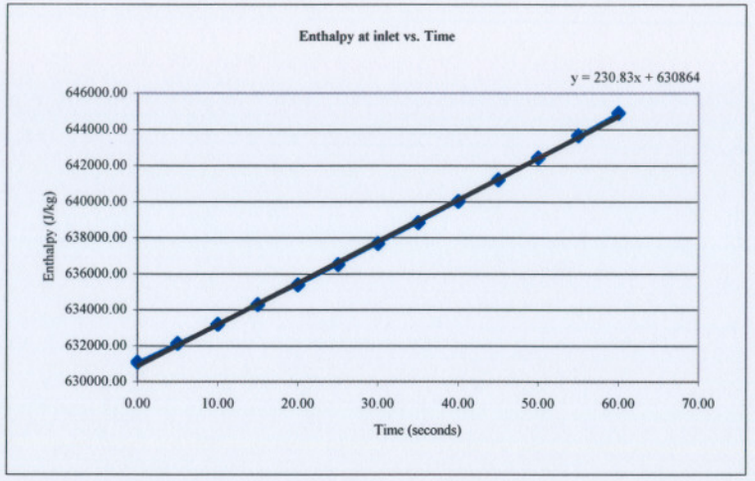

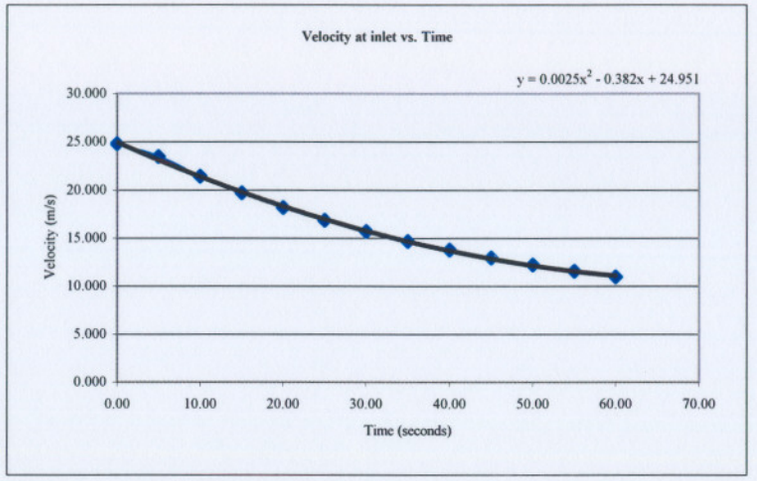

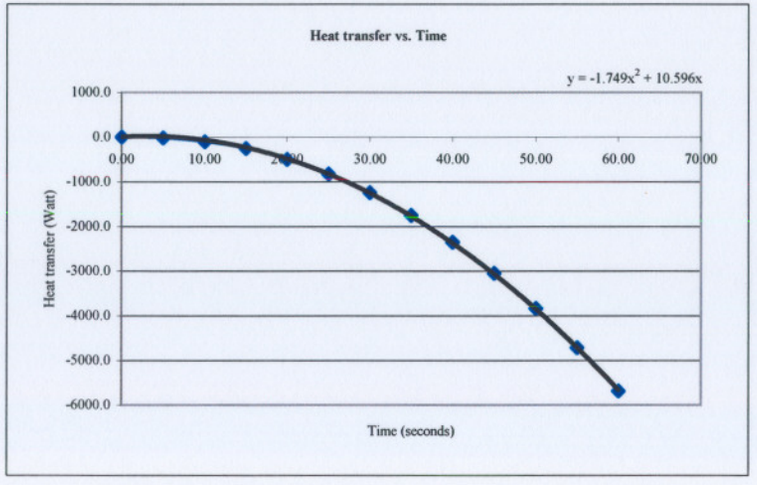

Model: Sensitivity (-10%)

Time seconds	Velocity m/s	Enthalpy J/kg	m.(hi+((vi)^2)/2)) J
0	24.951	630864	0.0
1	24.572	631095	5682570.4
2	24.197	631326	5684565.7
3	23.828	631556	5686563.3
4	23.463	631787	5688563.2
5	23.104	632018	5690565.3
6	22.749	632249	5692569.6
7	22.400	632480	5694576.1
8	22.055	632711	5696584.7
9	21.716	632941	5698595.3
10	21.381	633172	5700607.9
11	21.052	633403	5702622.4
12	20.727	633634	5704638.9
13	20.408	633865	5706657.2
14	20.093	634096	5708677.4
15	19.784	634326	5710699.3
16	19.479	634557	5712723.0
17	19.180	634788	5714748.3
18	18.885	635019	5716775.4
19	18.596	635250	5718804.0
20	18.311	635481	5720834.2
21	18.032	635711	5722866.0
22	17.757	635942	5724899.2
23	17.488	636173	5726934.0
24	17.223	636404	5728970.1
25	16.964	636635	5731007.7
26	16.709	636866	5733046.6
27	16.460	637096	5735086.8
28	16.215	637327	5737128.3
29	15.976	637558	5739171.1
30	15.741	637789	5741215.1
31	15.512	638020	5743260.3
32	15.287	638251	5745306.7
33	15.068	638481	5747354.1
34	14.853	638712	5749402.7
35	14.644	638943	5751452.4
36	14.439	639174	5753503.1
37	14.240	639405	5755554.8
38	14.045	639636	5757607.5
39	13.856	639866	5759661.2
40	13.671	640097	5761715.8
41	13.492	640328	5763771.4
42	13.317	640559	5765827.8
43	13.148	640790	5767885.1
44	12.983	641021	5769943.2
45	12.824	641251	5772002.1
46	12.669	641482	5774061.9
47	12.520	641713	5776122.4
48	12.375	641944	5778183.7
49	12.236	642175	5780245.7
50	12.101	642406	5782308.5
51	11.972	642636	5784371.9
52	11.847	642867	5786436.0
53	11.728	643098	5788500.8
54	11.613	643329	5790566.3
55	11.504	643560	5792632.3
56	11.399	643790	5794699.0
57	11.300	644021	5796766.3
58	11.205	644252	5798834.2
59	11.116	644483	5800902.7
60	11.031	644714	5802971.8

344545118	J	Sum[m.(hi+((vi)^2)/2))]
-106855	J	Q
344438263	J	Sum[m.(hi+((vi)^2)/2))]+Q

Model: Sensitivity (-10%)

FLUID - Internal energy deviation

Helium in Tank

Volume m^3		Temperature K	Gauge pressure Pa	Abs Pressure Pa	Avg density kg/m^3	Enthalpy J/kg	Mass kg	Internal energy J/kg	m.u J
100.390	start	293.00	0	3019000	4.96	113456.18	497.93	-495213.17	-246583428
	end	334.16	4126215	7145215	10.35	341315.18	1039.04	-349043.75	-362668838

m2u2-m1u1	J	-116085410

Helium in Pipe

Volume m^3		Temperature K	Gauge pressure Pa	Abs Pressure Pa	Avg density kg/m^3	Enthalpy J/kg	Mass kg	Internal energy J/kg	m.u J
0.979	start	293.00	0	3019000	4.96	113456.18	4.86	-495213.17	-2404365
	end	392.75	4126332	3019009	8.76	631066.25	8.58	286443.65	2456328

m2u2-m1u1	J	4860692

SOLID material - Internal energy deviation

Capacitance

Volume m^3		Temperature K	Density kg/m^3	Mass kg	Cp J/kg.K	m.Cp.T J
2.574	start	293.00	8030	20670.02	502.48	3043178035
	end	334.16				3470677038

m2u2-m1u1	J	427499003

Tank

Volume m^3		Temperature K	Density kg/m^3	Mass kg	Cp J/kg.K	m.Cp.T J
7.659	start	293.00	8030	61503.60	502.48	9054968500
	end	293.20				9061226626

m2u2-m1u1	J	6258127

Pipe

Volume m^3		Temperature K	Density kg/m^3	Mass kg	Cp J/kg.K	m.Cp.T J
0.056	start	293.00	8030	447.34	502.48	65859664
	end	385.97				86757183

m2u2-m1u1	J	20897519

Energy conservation

344438263	J	Sum[m.(hi+((vi)^2)/2))]+Q
343429931	J	Sum(m2u2-m1u1)
1008332	J	Difference
0.29	%	Deviance

Mass conservation

1042.79	kg	Initial mass + mass in
1047.61	kg	End: Density.Volume
4.82	kg	Difference
0.46	%	Deviance